TUHH
Hamburg University of Technology

Bachelor Thesis

Strain-gauge-based measurements of ice loads on ships

Till Zorn
Matr.Nr.: 21271674

handing in:
21 March 2018

Supervisors: Prof. Dr. Sören Ehlers, Dr. Rüdiger Ulrich Franz von Bock und Polach

Institute for Ship Structural Design and Analysis

Hamburg University of Technology

Abstract

Design loads are a central element of ship construction, because they influence plate and frame thickness. For the construction of ships that are destined to navigate in cold areas, it is extremely important to take into account the loads of ice impacts and their location on the hull. But ice is a particularly inconsistent material. To measure ice-induced loads, a lot of measurement has been undertaken, many of them used strain gauges. However, long-term strain gauge measurements are rare.

In this bachelor's thesis the state-of-the-art strain-gauge measurements are to be reviewed and problems with strain-gauge measurements will be discussed. Suggestions for improvement on problems like long cable complexity, big measurement setup, complicated installation, external power supply and long-term maintenance by humans while measuring will also be submitted.

Therefore, different systems and measurement possibilities should be compared in the context of long-term strain gauge measurements. A feasible solution for the mentioned problems, but also to identify the location and force of ice impact, will be designed.

Contents

1 Introduction

Design loads are a central element of ship construction, because they influence plate and frame thickness, as well as frame spacing and unassisted frame length. For the construction of ships that are destined to navigate in cold areas, it is extremely important to take into account the loads of ice impacts and their location on the hull. The knowledge about the size of these forces, their shape as a load patch and the duration of impact is an important factor in designing all supporting elements of ships. But ice is a particularly inconsistent material, which is not easy to understand. To measure ice-induced loads, a lot of measurement has been undertaken, many of them used strain gauges. However, most of the research contained short test runs, whereas long-term strain gauge measurements are rare.

Common measurement setups normally consist of strain gauges for measurement, connected via cables to amplifiers which send their data to a computer to be saved. This setup not only needs physical access to the questioned hull parts, but electric power supply, which again needs long cables. Maintaining such a setup is personnel-intensive and may obstruct the normal shipping process. Therefore, long-term measurements have some problems at that point.

Another problem is the attachment of long cables, which have to be plugged into an amplifier or the computer. The fast and easy configuration of the measurement system is also a problem of design. The work environment of ship structures are on the one hand also coming up with a lot of physical problems like humidity, cold temperatures, possibility of high speeds, accelerations and vibrations. On the other hand, there are difficulties for human beings to work there, because of little amount of space, darkness, humidity, air ventilation and transportation of measurement devices. Therefore, the installation of the measurement setup should be as easy as possible.

This paper compares different measurement systems in the context of strain-gauge measurement on ships. Possible solutions to the mentioned problems are suggested and the conceptual design of the best solution is to be identified.

2 Physical properties of ice loads and resulting measurement possibilities

When a ship comes into contact with ice, various physical properties play a certain role in the resulting outcome of an impact between them. Different methods of measurement use these properties or even add other effects and properties to get to a measurement result.

In this part, the analysis of the physical properties of ice loads will be considered. Those properties are important, as they affect the different measurement setups. The comparison enables us to identify and justify the choice of measurement setup. It will also give us an overview over older results to estimate the range-expectation of ice impacts.

2.1 Size range of ice loads/impacts and overview of older measurements

At first the size range of pressures of ice loads itself comes into focus of investigation. Because of the correlation of force and area defining the yielded pressure it should be clear that the assumption of load patches and the estimation of their area is crucial for the calculation of pressure. For load patches/areas see 2.2

Interesting for the size range of ice loads/impacts are upper and lower limits of the measured forces and pressures. One of the earliest ice-force measurements took place on R.V. Polarstern, when Hoffmann (1985) installed 'two triaxial force measuring devices [...] in pockets' (p.1190) (1,4 m × 0,8 m) with four load cells per device. He described the normal forces in level ice, pack ice and ice floes as similar. 'The highest value of normal force was measured with Fn = 2800 kN' (Hoffmann (1985), p.1194). One incident though was the destruction of one load cell due to a ramming impact of multiyear ice floes. It is only known that the load cell was capable of measuring up to 4 MN and that 'the area of impact exerted on this load cell is less the[n] 0,5 m^2' (Hoffmann (1985), p.1195). On CCGS Terry Fox, 'the peak single cell pressure was 11,3 MPa on an area of 0,12 m^2. The maximum total force measured was 5,0 MN' (Ritch et al. (2008), p.40). They made the assumption of a minimum cell pressure, as 'cells with pressures less than 0,25 MPa are considered to have zero pressure' (Ritch et al. (2008), p.36). The ice in this case was consisting of bergy bits with 'masses ranging from 30 t to 22 000 t, and the ship speed range was from 0,2 m/s to 6,5 m/s' (Ritch et al. (2008), p.30). At the same time (and on the same ship) Gagnon (2008)(p.58) was measuring forces of ice loads with the 'Impact Panel' (Gagnon (2001)) directly on the outside of the hull. The high peaks measured here were in a range between 14,9 MPa and 9,3 MPa. There was also the possibility to measure lower pressures, even though 'the sensor was not calibrated or designed for sensing in that low range but was able to indicate that pressure between 0 and 5 MPa' (Gagnon (2008), p.58). On PSRV S.V. Arghulas II the highest of the 'maximum ice loads [...] at manoeuvring tests' (Suominen et al. (2013), p.7) were just below 500 kPa. The tests were carried out 'in the northern part of the Bay of Bothnia' in 'one-year brackish water ice' (Suominen et al. (2013), n.p.). On the research vessel Araon Lee et al. (2014) were measuring peak pressures of 0,23 MPa to 2,12 MPa. Because of the summer time, four tests on ice floes were 'carried out in the Arctic Sea near Alaska, in the part surrounded

by Chukchi Sea and Beaufort Sea, between 73°N and 78°N' (Lee et al. (2014), p.790(3)). The length of the ice floes was between 130 m and 300 m and the width between 80 m and 110 m.

The values from the CCGS Terry Fox match pretty good with the results described so far. It is also reasonable to see higher loads at collisions with bergy bits than in level ice. Hoffmann (1985) measured values, which are a little bit lower in the median, but the case of the destroyed load cell leads to the assumption of a minimum pressure of $\frac{4\,\mathrm{MN}}{0{,}5\,\mathrm{m}^2} = 8\,\mathrm{MPa}$, which also fits in the measurements on CCGS Terry Fox, as this incident 'occured during the rammings with multiyear icefloes' (Hoffmann (1985), p.1195). On PSRV S.V. Arghulas II however, Suominen et al. (2013) measured significantly lower pressures, which might be the case due to the weaker ice conditions. The values measured on Araon are in between, but also comparatively low, especially in context of the ice floes estimated to consist of ice older than one-year old ice (cf. Lee et al. (2014), p.790). This is an observation, Ritch et al. (2008) and Gagnon (2008) made as well: 'there are general trends of higher pressure for larger bergy bit mass'. If that concept is also taken into account for level ice, assuming the older and thicker it is, the higher the pressure, my comparison of the outlined measurements fits into that scheme.

Surprisingly, Müller and Payer (1988)(p.499) found out, 'that the maximum loads were largely independent of the ship's speed'. Ritch et al. (2008)(p.46) also say that there is 'no discernable velocity effect', but Gagnon (2008)(p.64) says, 'there appeared to be a trend of increasing peak load with ship speed, however, the data exhibited a high degree of scatter (Fig. 23)'.

2.2 Area distribution of ice loads/impacts

The 1984 used pocket force measuring devices only made a pretty large assumption of local area of impacts possible. In case of the destroyed load cell, 'the area of impact exerted on this load cell is less th[an] $0{,}5\,\mathrm{m}^2$' (Hoffmann (1985), p. 1195). Yet, Müller and Payer (1988) discovered that, contrary to 'the uniform load of 9,5 MPa used for the dimensioning of the structure', 'the ice loads act as locally-confined impact loads for all ice conditions, i.e. also for the voyage in homogeneous sheet ice' (Müller and Payer (1988), p.499). Therefore, for the indication of peak stress in small areas, it is important to have a high resolution of strain measuring devices.

The smallest resolvable area of the mentioned trials was achieved by Gagnon (2008)(p. 51) with 'a unit sensing area [...][of] effectively $18\,\mathrm{mm} \times 18\,\mathrm{mm}' = 0{,}000\,324\,\mathrm{m}^2$. At strain-gauge measurement, there are two main strategies:

1. The measurement on the plate between the frames. (cf. Lee et al. (2014))
2. The measurement on frames with
   a) strain gauges at the end of the frame, close to the next higher supporting structure (cf. Suominen et al. (2017)) or
   b) distributed along the frame (cf. Müller and Payer (1988)).

Of course, these strategies can be combined, like Ritch et al. (2008) did. This was leading them to distinguishable load cells between 0,24 m^2 and 0,08 m^2 and to a total number of 120 strain gauges on nearly 4 m^2 instrumented area.

The detection of small, confined load-impact peaks can only be seen with high resolution, whereas the overall force per frame can be derived from the shear stress at the ends of the frame with much less strain gauges needed. This is a good ratio of reducing the number of measurement inputs vs. reduction of measureable information.

2.3 Duration of ice loads/impacts

To detect an impact (which can be a short moment in time) and to separately enregister it from a second one, measurement frequency is important. For that frequency, we need to know how long such impacts last.

An extreme impact happened 1984 on R.V. Polarstern, when 'the rise time of this impact was so short, that any statement about the force is impossible' (Hoffmann (1985), p.1195). The signals of the pocket force measuring device were processed 'with a rate of 50 Hz per channel' (*ibid.*, p.1190). Ritch et al. (2008) were using 500 Hz data collection rate – but afterwards, because 'noise was found to have components at various frequencies greater than 40 Hz', a 'low-pass filter with a cutoff of 30 Hz was then applied to all of the data' (Ritch et al. (2008), p.36). An example for an impact event is shown in Ritch et al. (2008), p.39, Fig.16, where most of this event is shown in the range of 0,35 seconds. For 0,2 seconds, the peak pressure builds up, after that, it decreases. 'Impact durations also corroborated for the two panels, i.e. in the range of 0,2-0,6 s' (Gagnon (2008), p.65). They used video cameras with a 'sampling rate' of '60 image fields per secong'(*ibid.*, p.54). On the Araon, the measurement system was using a 'sampling rate [of] 100 Hz and the rise time 'to the peak load [...] was measured as being 0.2-5 *sec*,' later it 'ranged from 0.2 *sec* to 0.5 *sec*. Also, 'there were some exceptions at around 1.0 *sec* [...] and at around 1.6 *sec*' (Lee et al. (2014), p. 792). Suominen et al. (2017)(p. 162) used 'sampling rates for [...] the strain gauge instrumentation [of] 200 Hz'.

The quickest rise times seem to range around 0,2 s, which relates to a frequency of 5 Hz. But a measuring frequency of 5 Hz would be insufficient because the pure detection of an impact is obsolete. The aim is to measure its load. To do that, measuring steps in between have to take place to get an image of the load curve. Therefore, at 30 Hz 6 steps would take place in 0,2 s. As this is the least sufficient, 10-12 steps like at 50-60 Hz would be good, 20 steps (100 Hz) is very precise, but comes with a high data flow, and might not be fail-safe to noise frequencies. 500 Hz are too much, noise is not needed. At the 200 Hz-system Suominen et al. (2017) give no information whether they had problems about noise or used any kind of noise suppression. So, depending on varying other factors, a measurement frequency between 30 and 60 Hz is recommended.

Another view on the needed measuring frequency is to look again on the ship's speed to estimate how fast a load would pass. An example for a polar ship can be the Araon, which has a 'Speed (*knots*, at 7,500kW)' (Kim et al. (2011), p.209) of 16,0 kn = $8,23\overline{1}$ m/s. To detect only an impact passing a structure like Suominen et al. (2017)(p.160) described (frame spacing = 0,4 m), strain gauges on every frame and a measuring frequency of

$\frac{8,23\overline{1}\,\frac{\mathrm{m}}{\mathrm{s}}}{0{,}4\,\mathrm{m}} = 20{,}578\,\mathrm{Hz}$ are needed. This is even lower than required in earlier measurements. A ship speed that high won't be able to be kept up and only be seen in a short period when just entering the ice at full speed. If such high speeds are not in interest, the 'Ice Performance (Design Target) Speed [of] $3knots$ in $1m$ level ice with flexural strength of not less than $630kPa$' (Kim et al. (2011), p.209) could be used for the frequency estimation. Then the minimum detection frequency even drops to $\frac{1,54\overline{3}\,\frac{\mathrm{m}}{\mathrm{s}}}{0{,}4\,\mathrm{m}} = 3{,}858\,\mathrm{Hz}$. It is important to note that this is only sufficient for the detection of this travelling impact. For a better insight in the run of the curve, again a much higher frequency is needed.

2.4 Slope of ice loads and differentiation between one impact and the next one

Gagnon (2008) showed in one example (p. 59, Fig 14) how the load behaves over time; the structure of the run of the curve can be seen and two peaks identified. The two peaks are identified as part of one impact, the first one mainly consists of crushed ice, the last one of hard ice. All of this takes place in $0,18\overline{3}\,\mathrm{s}$ or 11 time-steps, which corresponds to a measurement frequency of 60 Hz. The highest slope of this impact example was around $\frac{0{,}16\,\mathrm{MN}}{0,01\overline{6}\,\mathrm{s}} = 9,6\frac{\mathrm{MN}}{\mathrm{s}}$. To see this run and its rise with the two peaks, a measuring frequency of 30 Hz would have been insufficient and peaks may have been estimated lower because they were cut off. At Ritch et al. (2008)(p. 37, Fig. 14) small peaks occur in even smaller periods of time, whereas the main convexity of the run is much longer. This leads to the conclusion that, for an analysis of small (sub-)peaks following each other, a higher measurement frequency is needed, whereas for a slightly more imprecise result, the frequency can be reduced.

Considering again the context of the ship speed, the time, with which an ice load passes the load-patch width of 0,4 m, is $3{,}858\,\mathrm{Hz}^{-1} \approx 0{,}259\,\mathrm{s}$, which is longer than the the $0,18\overline{3}\,\mathrm{s}$ in Gagnon 's (2008) example of impact analysis. So it can be seen that the ship speed plays a small role in choosing the measurement frequency, because other effects need higher frequencies, if they are in focus of the measurement.

2.5 Differentiation between single and multiple ice loads/impacts

When it comes to multiple ice impacts along the hull, differentiation of them is important. With a method like the impact panel developed by Gagnon (2001) it is fairly easy to see areas of ship-ice contact directly on the small sensing areas under the acrylic glass slab. On a rigid plate, like the one Hoffmann (1985) installed on the R.V. Polarstern, the location of impact can only be estimated on the ratio of the force on the load cells. Smaller areas of identifiable load patches were implemented by Ritch et al. (2008) with a huge amount of strain gauges (frame spacing of 0,5 m, horizontal stringer every 0,4 m(*ibid* p. 31)). The basic principle behind this is 'the superponing principle', which is 'a result of the interaction between the frames' (Suominen et al. (2017), p. 155). This also works with higher frame lengths like 1,4 m (Suominen et al. (2017), p. 160). To detect the height of impact, the shear force can be determined from the shear stress, which can be fed into the calculation (cf. Suominen et al. (2013), p. 3) or FEA (cf. Suominen et al.

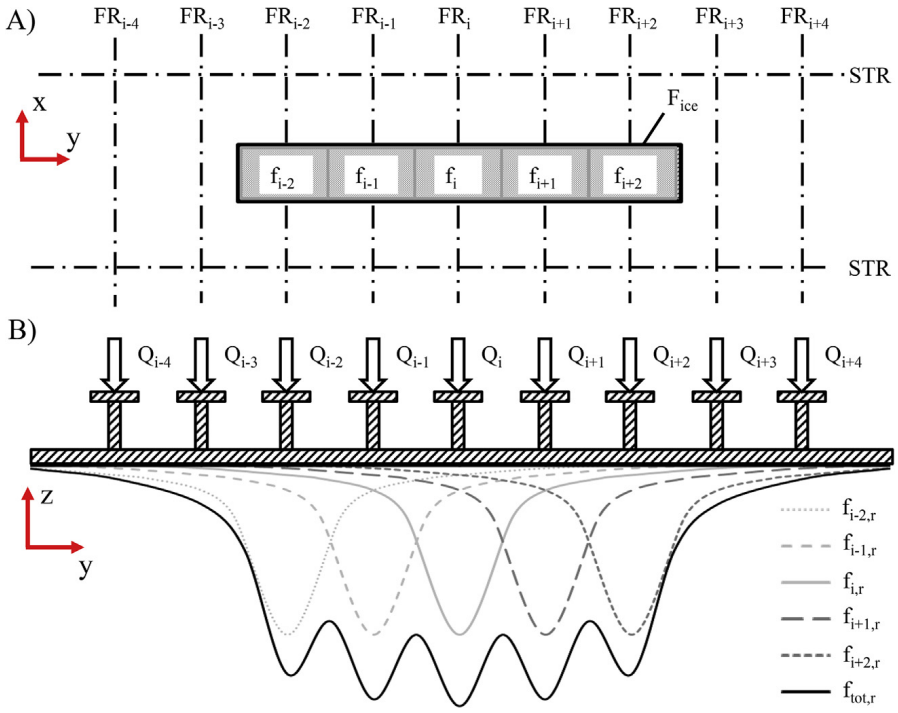

Figure 1: A) Ice load F_{ice} distributed into subloads f_{i+n} in the middle of frame (FR) and stringer (STR) grillage
B) Superposition of ice subloads f_{i+n} to f_{tot} and reaction forces Q_{i+n} of the frames
Figure taken from Suominen et al. (2017), p.156 Fig. 3

(2017), p. 155ff.). To detect the horizontal impact distribution several frames have to be equipped; the composition of 'an ice load [...] acting on the shell structure over several frames and its separation into subloads' provides insight into 'the horizontal length of the contact area' (Suominen et al. (2017), p. 156 Fig. 3 and 154). This can be seen in Figure 1 That requires a FEA of the structure to analyse the interaction of frames. This, of course, works not only on vertical structures, but on any frame which is in range of the expected ice load. At Ritch et al. (2008)(p.31, Fig. 4), the instrumented grillage can be seen. Vertical and horizontal frames have strain gauges at their ends and some have an additional one in the middle. The small frame and stringer spacing, combined with the massive use of 120 strain gauges, make the load cells on CCGS Terry Fox that small.

The instrumented area and the usage of strain gauges depends on the supporting structure. Longer supporting stiffeners allow a smaller amount of strain gauges used, but might not be as accurate as more strain gauges on a structure with more intersections between stiffeners. At this point, the impact panel of Gagnon (2001) is more elegant and precise in directly taping these impacts on video.

2.6 Duration of measurement

Suominen et al. (2017)(p. 164) were taking measurements 'in [...] the Baltic Sea on March 21-22, 2012' where '[a]pproximately 24 h' worth of data was collected'. The measurement on Araon consisted of four single measurements (cf. Lee et al. (2014), p. 791, Table 1). On CCGS Terry Fox, Ritch et al. (2008)(p. 30) conducted a 'total of 178 test runs', while Gagnon (2008)(p. 56) could only use 7 of a 'total of 42 impact experiments [which] showed something on at least one of the five functioning video cameras'.

2.7 Location of measurement zone on the hull

In most of the full-scale trials, those zones on the ship were equipped, where the strongest forces were expected. Therefore, it is reasonable to choose the bow area as measurement area. Mainly two positions at the bow were equipped, the bow shoulder, and an area some distance further ahead, e.g. the two pocket measuring devices (Hoffmann (1985)) on R.V. Polarstern, as well as the impact panel (Gagnon (2008)) in the front and the strain-gauge panel by Ritch et al. (2008) on the shoulder of CCGS Terry Fox. Hoffmann (1985) also put his force-measuring device on the bow and the bow shoulder. However, Müller and Payer (1988) instrumented a larger area, containing the earlier by Hoffmann (1985) eqipped sites. Suominen et al. (2013) additionally equipped the aft shoulder (can be seen in Figure 2), which also can be heavily loaded in some conditions such as breaking out from the channel (Suominen et al. (2013), p. 7).

In contrary to the above, the concept of measuring the strain within a structure is obviously not restricted to these areas. But some other measurement methods have restrictions or are very cost-intensive to implement on some parts of the ship. The impact panel by Gagnon (2001) is flat, so it would be very difficult to get it to work on curved or cone shaped hull parts. Even the pocket-measuring device that Hoffmann (1985) used can only measure at 4 spots, which are all highly influenced by each other due to the connection by the steel panel itself. This change of the ship structure might influence the outcome of the measurement. The different load cells identified at a strain-gauge measurement also influence each other, but its the structure itself, which is used for the measurement, so it is not influenced by any other interaction. That makes it easier to measure at any part of the hull with this method, but the calculation effort might be greater.

The height of the instrumented area is also crucial in order to measure on the same height as the ice is in contact with the ship. Müller and Payer (1988)(p.498) wrote 'that due to rolling and trim of the ship during ice breaking and ramming, the instrumented section frequently emerged and experienced impacts only occasionally'. Therefore, the instrumented area has to be long enough in the vertical direction, as it can be seen in Suominen et al. (2013), p.3, Fig. 1 (here reproduced as Figure 2, p.13). At the bow area, due to heave and pitch motion caused by the ship sliding up the ice before breaking, a slightly lower measurement location might be working without loosing data. This location of measurement area can bee seen at Ritch et al. (2008), p.30, Fig. 1. Both of the two panels (strain gauges and Impact Panel) are more below the waterline than

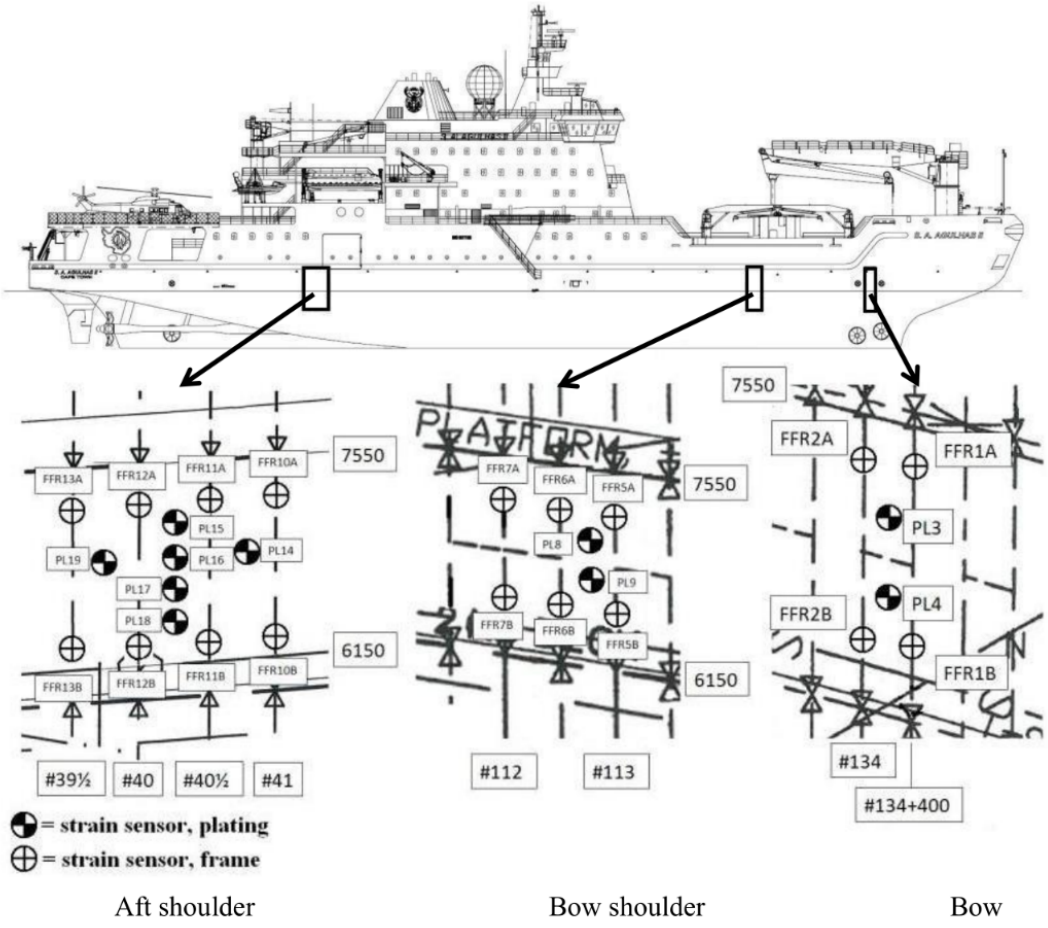

Figure 2: Common zones for measurement of ice loads, exemplary on S.A. Aghulhas II
A combination of strain gauges on frames and plate are used.
Figure taken from Suominen et al. (2013), p.3, Fig. 1

above.

2.8 Installation of measurement setup

The different measurement setups not only prefer different measurement locations on the hull, but some also need modifications of the hull. The biggest changes are needed for the triaxial force measuring device, as it has to be installed in pockets, which need to be cut out of the hull. Then, there has to be built a pocket behind that cut-out, which is then filled with the load cells and the top plate on top (cf. Hoffmann (1985), p.1190f., Fig. 2). There can also be seen a pipe from the pocket upwards, which is, to my consideration, used in means of pressure balance and cable run (Hoffmann (1985) gives no further explanation).

The Impact Panel of Gagnon (2008) consists of layers of mirror sheet, acrylic slab and

a stainless steel sheet and is surrounded by a box channel with cameras inside (*ibid.*, p.52, Fig. 6). This rests on a 'Mounting Bracket' and is surrounded by 'faring plates' (*ibid.*, p.54), which had been welded to the hull. Also the cables were put into a conduit, which was also welded up to the bulwarks. Therefore, also the impact panel needs a (albeit smaller) modification of the hull by welding on it.

Strain gauges however, are installed inside of the hull. Most likely, they are glued, but can also be welded onto the surface. This features flexibility and easy installation, but requires access to a continuous room near the waterline per measuring section which isn't filled while measuring. Power and measurement cables require connection to a power supply and data storage, if not contained in situ.

2.9 Differentiation between ice loads and other impacts

At first, when it comes to general loads on the hull, wave slamming comes into mind. Therefore, I made a simple estimation of wave pressure by using the 'design bow impact pressure' of the DNV GL class documents (2017) at a location close to the waterline in the front bow. The resulting pressure of $P_{FB} = 591{,}939\,\text{kPa}$ is even higher than Suominen et al. (2013) measured in level ice, but lower than high peaks of other measurements. The design bow impact pressure is also only the maximum of any assumed wave pressure. Since not only the peaks are interesting, there might be a problem with keeping them apart from ice impacts on long-term journeys with a ship's operational profile of both, open and ice-covered waters. In case of mixed conditions like a broken channel, ice loads are again interesting and waves can be assumed to be nonexistant or very small.

The easiest solution is to analyse on-board documentation of the journey with the exact time of entering and leaving ice covered waters and correlate the time to the measuring unit. This correlation might be a problem, if the two clocks are left without connection over a longer measuring period, respectively increases the standards on them.

The other possibility is the differentiation only on basis of the measured data. Therefore, the total amount of load might be the first indication. Further ones could be the different load patch or load length, as well as the different impact height from the waterline. The speed with which the impact passes the ship might be the strongest characteristic of differentiation, as a ship in open waters is most likely faster than in ice.

Another example for impacts similar to ice impacts might be a collision. This can range all sizes. Smaller collisions, e.g. with flotsam, might not turn up on the ship's log, whereas bigger collisions, which also may cause damage, will turn up on the log, which can make interpreting the data easier. A collision should also be a one time contact, so a single peak would most likely be such a collision.

Further analysis of this particular problem could be the subject of another paper.

2.10 Resulting measurement possibilities

Three main systems of measurement are reviewed so far:

1. 'force measuring devices [...] in pockets' (Hoffmann (1985), p.1190) on R.V. Polarstern

2. 'Impact Panel' (Gagnon (2008), resp. Gagnon (2001)) on CCGS Terry Fox

3. strain gauges on inside of the hull (different strategies, cf. 2.2).

All of them are capable of measuring impacts, of course, but other qualities differ from one another. First of all, the quality of the measured data itself is important. The Impact Panel is the most precise device in locating an impact, the force measuring device on R.V. Polarstern the least precise. With strain-gauge measurement, precision depends on the number of strain gauges used. The measurement frequency, even at the upper limit of what is needed, can be achieved with all of the systems, modern cameras, as well as strain gauges. The raw data analysis of strain gauges starts with numbers, which might be easy, but a FEA has to be made in order to interpret the data. At the video data from the Impact Panel an 'image-by-image analysis' (Gagnon (2008), p.56) is needed. Both comes with some effort. Very little effort is needed at the raw data from R.V. Polarstern, as there is not much data and it is already easy to interpret.

The differentiation of loads is fairly easy with the images from the video, but after calculating the FEA model, strain gauges can also be good at that, but they are just not as precise. The force-measuring device, however, only measures the forces on the top plate of the device, therefore differentiating the impacts is very imprecise resp. not possible.

Since the aim is to measure self-sufficient, a lot of raw data has to be stored, and even more so in means of video data; the more data is produced, the more has to be stored until analysing. When it comes to data efficiency, the videos, which the Impact Panel produced, were often insufficient due to various problems (cf. Gagnon (2008), p.55f). This makes date efficiency of the Impact Panel even worse. Therefore, strain-gauge data is more attractive.

This applies also to the flexibility of possible measurement locations on the hull. Strain gauges are more flexible in size and location of the questioned load patch. The Impact Panel requires a flat surface and is restricted in size. As curved shapes might be possible at the R.V. Polarstern's pockets, the size needs a corresponding support structure underneath, which might be difficult to realize.

Similar problems with the Impact Panel and the Pockets occur in the installation. Both need welding, which means a change in the ship structure, additional equipment and maybe even docking of the ship.

On the one hand, high precision in impact sensing, like from the Impact Panel, is important, indeed, but this doesn't outweigh the disadvantages in other fields. On the other hand, the force-measuring device on R.V. Polarstern is definitely not precise enough and, on top of that, has even more disadvantages. Therefore, strain gauge measurement is the compromise of choice for this task. The exact implementation is discussed in the following.

3 State-of-the-art strain-gauge measurement

The measurement of stress over strain has a long history in measurement technology. The measurement approach with strain gauges - electrical resistors changing their resistance as they are lengthened - was first developed in 1936 (Keil (2017), p.1). Today, they are an indispensable tool of stress and strain measurement. Many characteristics of strain gauges have to be understood in order to design the whole measurement system. However, the only means discussed will be the ones relevant for the purpose of this thesis.

3.1 General

The basic idea of strain-gauge measurement is to attach an electrical resistance - which is, due to its material and structure, resistance-sensitiv to strain - to the device under test (cf. Simmons (1942)). The strain gauge sits in an electrical driven system, called Wheatstone bridge, which changes its output voltage when the electrical resistance of the strain gauge changes (cf. Ruge (1944)). The output voltage is then amplified and the thus produced measurement signal is displayed and/or recorded. A diagram of this can be seen at Figure 3. By applying the specified conversion factors of the several steps, the strain and, depending on the installation strategy of the strain gauges, the stress can be calculated from the output data.

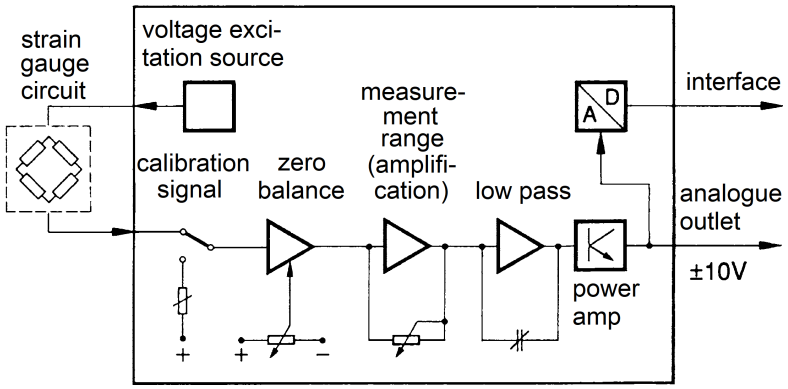

Figure 3: Concept of analogue measurement system with A/D-converter and digital output
Figure taken and translated from Keil (2017), p.215, Fig. 7.1

3.2 Structure of strain gauges

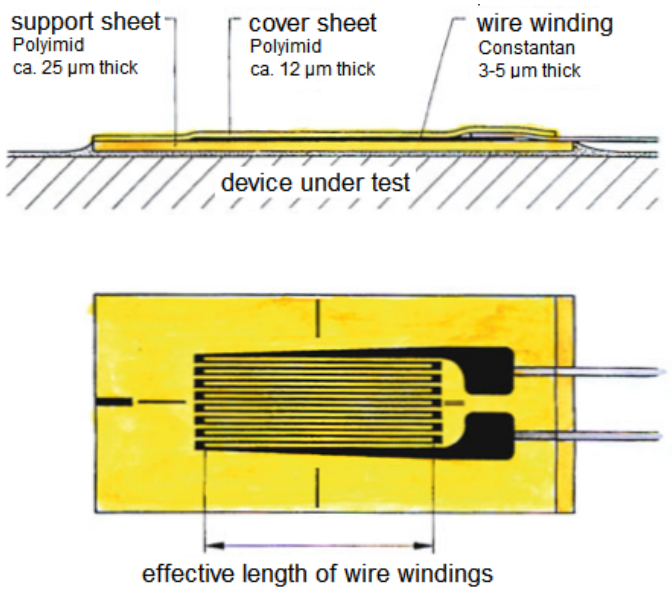

Figure 4: Modern sheet based strain gauge
Figure taken and translated from Keil (2017), p.15, Fig. 2.2

A strain gauge consists of multiple windings of wire on an electrical isolating support. The wire is made out of a material, which changes its ohmic resistance when it is stretched or compressed. Over the change of this resistance a change in strain of the wire can be measured. The change in ohmic resistance $\frac{\mathrm{d}R}{R}$ equals the strain ε over a proportionality factor called k:

$$\frac{\mathrm{d}R}{R} = k\varepsilon \tag{1}$$

In order to get the strain of the device under test, the wire windings have to be attached to it. As the measurement uses electricity, the wire windings need to be electrically insulated, but mechanically connected. In the past, paper was used as support material (cf. Simmons (1942) and Ruge (1944)). The evolution of support materials soon went form paper to plastics, because of the requirements of good mechanical transmission even in thin slices, whilst having enough electrical insulation to not distort the measurement, even in humid environments. Other requirements are flexibility, compatibility with glues, handling and others. As plastics can be adjusted for different purposes, synthetic resins were used first, whereas modern plastics, such as polyimid (Keil (2017), p.26ff.), are the material of choice today. Strain gauges that are metallic or ceramic supported exist, but are peripheral for this paper, since they are made for special-purposes.

The connection with the device under test is mostly done with special glues, which also have to satisfy the requirements mentioned above. In this way, the mechanical connection

of wire and the device is made. As a cover on top of it, a thin plastic layer protects the wire windings from above. The composition of that can be seen in Figure 4

As wire material, mostly alloys are used. The usage of an alloy depends on its own physical properties, in regard to the different environmental properties, in which the strain gauge will be used. Important properties are the temperature behaviour, the specific resistance influencing the size of the wire windings, the vibration resistance and the resistance sensitivity of strain influence. Constantan is one of the most-used wire materials followed by Ni-Cr-Alloys (cf. Keil (2017), p. 28.ff.). Some of the properties will be discussed in the following, since they play a role in choosing the parts of the measurement system.

3.3 Temperature changes

The temperatures on ships can vary, especially over a long period of time. Differences in draught or heaving can mean a drastic difference on the outside of the ship, as maybe fluid seawater around 0 °C or cold arctic air and ice touch the hull. Since steel is a good heat conductor and the measurements in question take place around the waterline, where these changes will most likely occur, the strain gauges also need to cope with these temperature changes. Therefore, this is an important environmental influence. Several temperature phenomenons can lead to a change in the resistance of measured strain gauges:

First, the proportional factor k can be influenced by different temperatures. Keil (2017) (p.45) gives a linear correlation between the change in k-factor and the temperature within a certain temperature range. This leads to

$$\frac{\Delta k}{k} = \alpha_k \Delta T \tag{2}$$

With a reference temperature of $T = 20\,°\mathrm{C}$ an example in change is given in Figure 5. The ratio seems also to be dependant on the glue used for attachment.

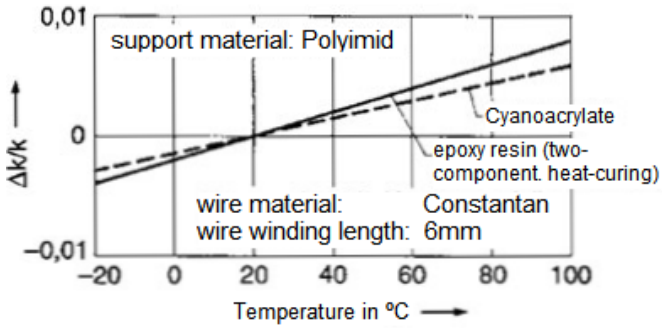

Figure 5: k-factor change over temperature
Figure taken and translated from Keil (2017), p.45, Fig. 2.31

The second effect is the overall electrical resistance of the wire material used in the strain gauge, which changes depending on the temperature. This can be avoided by using

materials like constantan, but not all wire materials have properties like that. A zero balance is not possible, as the measurement temperature might change during the long measurement period. A temperature data logging for all the temperatures at the hull locations in question, would most likely be too much effort.

The third effect is a difference in the temperature lengthening of wire and measurement material. As one material stretches or shrinks more than the other, the effect on the strain gauge is like every other strain ε. This leads to an offset in the measured data. The second and third effect can be summed up (Keil (2017), p.45ff.) as follows:

$$\left(\frac{\Delta R}{R_0}\right)_{\text{therm}} = \alpha_R \Delta T_{20} + k_T(\alpha_B - \alpha_M)\Delta T_{20} \tag{3}$$

To encounter these temperature influences, Keil (2017)(p.46f.) states two main compensation methods:

The first is to use a dummy strain gauge in the wheatstone bridge. The wheatstone bridge compares the ratio of two (resp. four) ohmic resistances. If the temperature effect acts on both resistances, the ratio stays the same and temperature errors are therefore cancelled out. To realize this, the compensation gauge has to be installed on a strip of the same material at the same measurement location. This strip must not be connected mechanically, but only thermal. This can be achieved with a strip of the same metal, which is attached with one end near the measurement location of the original strain gauge, while the other end is free (cf. Keil (2017), p.147ff.).

The second method is to use self-compensated strain gauges. These work only with one underlying material, as they use the second against the third effect. The differences in lengthening and ohmic-resistance change are cancelled out when, due to the right choice of wire material, both effects are changing the electrical resistance in different directions and at the same absolute value. The error caused by non-linear behaviour of the two different effects can be assumed reasonably small.

3.4 Creeping as long-term influence

The connection between the device under test and the wire windings is crucial. At this point, the used adhesive is an important part, but also the long-term behaviour of this compound, as creep influence might be a problem. Creeping can also be an effect of the strain gauge itself, as the force transmission between wire and plastic inside the gauge can be not ideal due to environmental conditions.

The influence of creep is in this respect important, as not long-term forces cause deformation, but temperature changes, which might occur over long periods due to weather changes. Another reason for creep could be a permanent deformation caused by collision or thicker ice than accounted for in the ship design. Therefore several factors of creep need to be discussed:

- the duration
- the temperature

- dimensions of the wire windings
- the tapping of the wire windings
- creeping of the device under test

(cf. Rohrbach and Czaika (1960) and Keil (2017)(p.52ff.))

The biggest influence on creeping is the temperature and the duration, since the device under test is being lengthened and the strain gauge can adapt to it. Over the time, this strain deviation (also called relative strain $\frac{\Delta\varepsilon}{\varepsilon}$) is assumed to follow an exponential form with a certain limit. As a total relaxation and therefore a deviation of 100 % is only seen at higher temperatures, at lower temperatures the relative strain stays pretty low. But as Rohrbach and Czaika (1960) say, the strain deviation in form of an e-function covers the data only for shorter time periods. It is to mention that the lowest temperature, at which Rohrbach and Czaika (1960) were measuring strain deviation, was room temperature, respectively 20 °C.

Some of the graphs at Rohrbach and Czaika (1960) show an e-function-like behaviour at 20-25 °C, others seem to adapt a small but steady rise in strain deviation (cf. Figure 6). Therefore, this behaviour might also occur at even lower temperatures like on the inside of an icebreaker hull. As aiming for long-term installation this might influence the overall measurement. Therefore the effect has to be eliminated in the calculation or at the measurement itself.

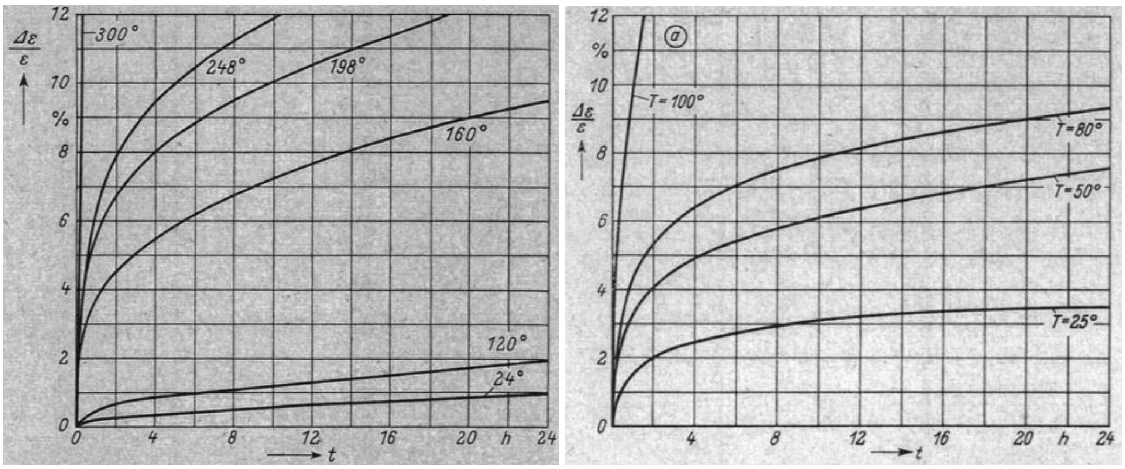

(a) Slowly rising relative strain at 24 °C
figure taken from Rohrbach and Czaika (1960), p.37

(b) e-funktion like graph at 25 °C
figure taken from Rohrbach and Czaika (1960), p.55

Figure 6: relative strain $\frac{\Delta\varepsilon}{\varepsilon}$, temperature in ° (Celsius)

Keil (2017)(p.55f.) states that many other factors are also involved in creeping of strain gauges. One of the bigger influences is the length of the wire windings, the longer these are, the less creeping occurs. Another influence, that Keil (2017)(p.57ff.) names is the creeping of the device under test itself. He tells about a solution of the creeping

problem, because the creeping of the device under test goes in the opposite direction than the relative strain. Therefore strain gauges that are adjustable in length could be set up to a length where both influences cancel each other out.

This solution can only be used, when the static strain in the material is caused by an external force or a deformation. As static forces don't appear, a deformation by a big force is the only incident, when this approach would be useful. Therefore, this is to be kept in mind for the design, if the effort is worth it. The creeping problem of temperature lengthening can also be resolved by placing a dummy strain gauge in the wheatstone bridge, as discussed in 3.3.

3.5 Installation of strain gauge

The installation of a strain gauge has to follow many steps. Keil (2017)(p. 109) gives 9 main steps with the example of cyanoacrylat:

1. roughening after removing the grease
2. final cleaning
3. marking of the strain gauge position
4. positioning of strain gauge
5. applying the adhesive
6. adhesive distribution with teflon strip
7. pressing the strain gauge on top
8. soldering of cable to strain gauge
9. covering after flux removing

First of all, the material surface of the device under test, in our case the ship hull, has to be free and even. Keil (2017)(p.103f.) recommends sandblasting as roughening, but mentions also sandpaper as sufficient tool.

Keil (2017)(p.107ff.) also gives an overview of commonly used attachment methods and compares their qualities. He gives cyanoacrylate as material, which is mostly used in present strain-gauge installation on metals (cf. *ibid*, p.108). On the other hand, he states two problems with cyanoacrylat: because of the liquidity of the adhesive, applying it on a sloped area is difficult; and he does not recommend it for long-term installation. Additional to that, he gives the temperature range of cyanoacrylat with $-30\,^{\circ}\mathrm{C}$ to $100\,^{\circ}\mathrm{C}$. The lower limit can be reached on the outside of the hull of an icebreaker in operation.

With a temperature range of $-200\,^{\circ}\mathrm{C}$ to $50\,^{\circ}\mathrm{C}$, methylacrylat adhesives cover the needed range better. It is said to be ropy and should therefore be applyable to sloped areas. Keil (2017) also points out the dual use for not only the strain gauge itself, but also for cables and sheet metal for compensation gauges etc. (cf. p.111).

Resin-based adhesives have similarly good properties, but most of them need increased temperatures in order to get the hardening agent to work (cf. Keil (2017), p. 111). This might be a problem, because the thick icebraker hull is a good heat sink and much power (e.g. for induction heating) or additional instruments (like flame torches and thermometer) are necessary. Other methods like welding, ceramic adhesives or flame spraying can only be mentioned here, but are too complex for this task and therefore not discussed.

The protection of a measurement location can vary due to environmental conditions. As for the easy installation, the room has to be accessible. This leads to the assumption of a void space between hull and supporting structure. A room like this is already protecting the measurement equipment from many environmental influences, but dust, humidity or even a little bit of dripping or condensing water at the outer hull (due to the cold temperatures) might be possible. Keil (2017) gives some requirements. The protection cover should jut out over the strain gauge and the tapping by 10 mm to 20 mm (cf. *ibid*, p. 131) and should be applied soon after the installation of the strain gauge itself, in order to minimize the impurity trapped underneath. Therefore, the measurement location also needs to be completely dry, as the aim is to keep humidity away. Keil (2017) mentions also the cable as a critical point in covering, as it has to be covered from all sides, also from below (cf. p.131). For long-term measurements, the protection ought to consist of several layers of different covers (cf. *ibid*, p. 133ff.).

3.6 Vibration and impact stress

Generally, strain gauges are, 'because of their small mass, [...] predestined for dynamic strain measurement' (translated from Keil (2017), p.75). However, vibration and oscillation over a longer period in time can damage a strain gauge. According to Keil (2017) this is interdependent to the number of load cycles, as well as to the amplitude of vibration. The higher the amplitude, the sooner a shift in the zero signal occurs. As the amplitudes from ice impacts are much smaller than the ones given by Keil (2017)(p. 76, Fig. 2.56), vibration is not important for the strain gauges.

3.7 Energy consumption and waste heat

Since an autonomous measurement system for a long time is to be designed, two things are important to consider, when it comes to energy consumption:

- the total amount of energy used for the measurement has to be stored at the measurement system and
- the waste heat produced by the strain gauge while measuring, which could cause measurement errors.

Chalmers (1992) gives a table for 'allowable gauge power dissipation' (p.30) at different accuracies for static and dynamic measurements. He says, 'when purely dynamic signals are involved, minor instability and drift are relatively less important, so that considerably

higher power levels can be employed' (Chalmers (1992)(p.29)). This of course depends on the material of the device under test as well as on its thickness, because it serves as a heat sink. The values are given in kilowatts per square meter, respectively milliwatts per square millimetre, which takes into account that larger strain gauges can spread their energy better and therefore don't heat up that much (cf. to Table 1).

Accuracy	thick steel	thin stainless steel
High	7,8-16	3,1-7,8
Medium	16-31	7,8-16
Low	31-71	16-31

Table 1: Excerpt for good and fair heat sinks at dynamic signals from Chalmers (1992), p.30, table 4: 'allowable gauge power dissipation in [...] kilowatts/m^2' Note: $\frac{\mathrm{kW}}{\mathrm{m}^2} = \frac{\mathrm{mW}}{\mathrm{mm}^2}$

The power of a single strain gauge P_{sg} is given by

$$P_{sg} = \frac{U_B^2}{4R} \tag{4}$$

and therefore the power density P'_{sg} by

$$P'_{sg} = \frac{U_B^2}{4RA}. \tag{5}$$

Because a possible temperature compensation, as discussed in 3.3 and 3.4, would be installed on a thermally connected sheet of the same material, their thickness most likely would not be the same (cf. Keil (2017), p.147ff.). Therefore, the difference in the quality of the device under test and of the compensation sheet, as heat sinks, has to be kept in mind as it might influence the accuracy of the measurement.

As an example, with the commonly known formulas for electric current I, resistance R, voltage U and power P

$$U = RI; \tag{6}$$

$$P = UI = RI^2 = \frac{U^2}{R}, \tag{7}$$

common strain-gauge resistances and voltages cause different power consumptions P_{sg}, needed areas A_{ne} and energy consumptions E_{4w} (over 4 weeks nonstop measurement): For the area calculations, $P' = 16$ was assumed for thick steel and a high accuracy. The high-limit value was used in order to get a lower limit at the area calculation. (4) and (5) result in

$$A_{ne} = \frac{P_{sg}}{P'_{sg}} \tag{8}$$

As example for a long-term measurement, 4 weeks were assumed. Therefore, the energy consumed by one strain gauge is

$$E_{4w} = P_{sg} \cdot t. \tag{9}$$

Resistance / Voltage	120 Ω	350 Ω	700 Ω	1000 Ω
0,5 V	$P_{sg} = 0{,}521\,\mathrm{mW}$ $A_{ne} \geq 0{,}033\,\mathrm{mm}^2$ $E_{4w} = 0{,}350\,\mathrm{Wh}$	$P_{sg} = 0{,}179\,\mathrm{mW}$ $A_{ne} \geq 0{,}011\,\mathrm{mm}^2$ $E_{4w} = 0{,}120\,\mathrm{Wh}$	$P_{sg} = 0{,}089\,\mathrm{mW}$ $A_{ne} \geq 0{,}006\,\mathrm{mm}^2$ $E_{4w} = 0{,}060\,\mathrm{Wh}$	$P_{sg} = 0{,}063\,\mathrm{mW}$ $A_{ne} \geq 0{,}004\,\mathrm{mm}^2$ $E_{4w} = 0{,}042\,\mathrm{Wh}$
1 V	$P_{sg} = 2{,}083\,\mathrm{mW}$ $A_{ne} \geq 0{,}130\,\mathrm{mm}^2$ $E_{4w} = 1{,}400\,\mathrm{Wh}$	$P_{sg} = 0{,}714\,\mathrm{mW}$ $A_{ne} \geq 0{,}045\,\mathrm{mm}^2$ $E_{4w} = 0{,}480\,\mathrm{Wh}$	$P_{sg} = 0{,}357\,\mathrm{mW}$ $A_{ne} \geq 0{,}022\,\mathrm{mm}^2$ $E_{4w} = 0{,}240\,\mathrm{Wh}$	$P_{sg} = 0{,}250\,\mathrm{mW}$ $A_{ne} \geq 0{,}016\,\mathrm{mm}^2$ $E_{4w} = 0{,}168\,\mathrm{Wh}$
5 V	$P_{sg} = 52{,}083\,\mathrm{mW}$ $A_{ne} \geq 3{,}255\,\mathrm{mm}^2$ $E_{4w} = 35{,}000\,\mathrm{Wh}$	$P_{sg} = 17{,}857\,\mathrm{mW}$ $A_{ne} \geq 1{,}116\,\mathrm{mm}^2$ $E_{4w} = 12{,}000\,\mathrm{Wh}$	$P_{sg} = 8{,}929\,\mathrm{mW}$ $A_{ne} \geq 0{,}558\,\mathrm{mm}^2$ $E_{4w} = 6{,}000\,\mathrm{Wh}$	$P_{sg} = 6{,}25\,\mathrm{mW}$ $A_{ne} \geq 0{,}391\,\mathrm{mm}^2$ $E_{4w} = 4{,}200\,\mathrm{Wh}$

Table 2: Overview of results of sample calculations to show limits and possibilities of power consumption, heat generation and voltage, calculated with DC voltage

From Table 2, we can see pretty low area limit values, even at this high accuracy. As the structural elements of an icebreaker are thick, the area is no limit at this point. The power consumption however is a more critical point, due to the requirement of long-term measurement. Even an apparently low electric current like 52,083 mW consumes without any losses, and without the measurement system, which needs additional power, 35 Wh. This leads to the conclusion of saving power by using less consuming strain gauges and/or a low voltage to get a self-sufficient system.

Compared with the power consumed by the amplification and computer-control unit (see 5.2), the strain gauges need a minor amount of energy. In tests of the measurement system prior to the measurement on board of an icebreaker, it should be tested, how big the effect of strain-gauge-power consumption on the complete measurement system really is.

4 Measurement system and its required parts

This chapter will take a look in the electronics of the measurement system. The aim is to define the boundaries in which a system can operate and which properties are required. It will lead to the design of all parts and to the comparison of buildable and buyable components.

4.1 Wheatstone bridge

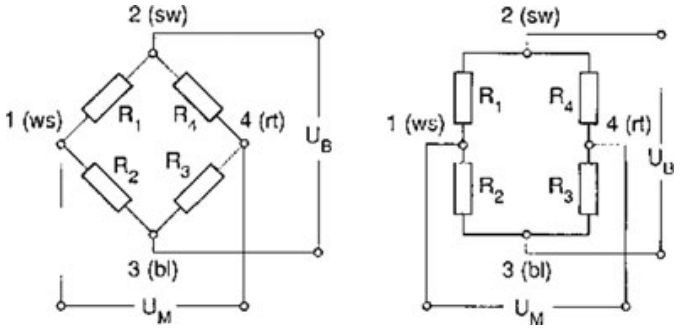

Figure 7: Two depictions of the wheatstone bridge
$R_1 ... R_4$: Resistors of leg 1...4
U_B: bridge supply voltage
U_M: measured voltage
2 and 3: node for bridge-supply voltage
1 and 4: node for measured voltage
Figure and description taken (and translated) from Keil (2017), p.142, Fig. 4.1

The wheatstone bridge (see Figure above) is a well-known, often-used measurement method for ohmic resistance. The principle of the circuit is to compare the output voltage of two parallel voltage dividers. If realised with strain gauges, in the initial state, all resistances are equal, and therefore the measured voltage is zero (balanced wheatstone bridge). If a resistor changes its resistance, the electric potential between the two resistors of that branch changes, which results in a measurable voltage between node 1 and 4 (unbalanced wheatstone bridge). Additional to that the measured voltage is linearly dependant to the bridge supply voltage (cf. Keil (2017), p.141f.).

To analyse the interdependencies mathematically Keil (2017)(p.142) gives the formula:

$$\frac{U_M}{U_B} = \frac{R_1}{R_1 + R_2} - \frac{R_4}{R_3 + R_4} \tag{10}$$

The assumption made, is to have a high-impedant voltage measurement and therefore the electric current between node 1 and 4 is negligible. It can be seen, that $U_M \sim U_B$ and resulting out of this, the ratio $\frac{U_M}{U_B}$ is independent of U_B itself.

Based on (10), Keil (2017)(p.143) defines the nominal resistance of each strain gauge as $R_0 = R_1 + R2 + R_3 + R_4$ and the change of resistance in each branch as ΔR_i. As these

changes are very small compared to the resistance, the multiplication of two of them is assumed to be negligible, which leads to the basic equation of the wheatstone bridge (cf. *ibid*, p. 143):

$$\frac{U_M}{U_B} = \frac{\Delta R_1 - \Delta R_2 + \Delta R_3 - \Delta R_4}{2(2R_0 + \Delta R_1 + \Delta R_2 + \Delta R_3 + \Delta R_4)} \tag{11}$$

Keil (2017)(p. 144) gives an even more simplified version of this equation for metallic materials within the elastic deformation. Keil (2017) gives the approximation only for one resistance and later superpones these for strain calculations. The approximation assumes $\Delta R_i \ll R_0$, which leads to the complete equation

$$\frac{U_M}{U_B} = \frac{\Delta R_1 - \Delta R_2 + \Delta R_3 - \Delta R_4}{4R_0} \tag{12}$$

This equation shows us, how to intensify the measured voltage by placing the strain gauges cleverly. As the device under test undergoes a force, strain occurs, at some locations positive, at other locations negative. If two strain gauges of the same branch of the wheatstone bridge (e.g R_1 and R_2) are placed on such interdependent locations, they both add up, which increases the measurement signal (cf. Keil (2017), p. 144).

Another advantage that can be used is the compensation of effects of parasitic drag, which influences the whole circuit (cf. Keil (2017), p.143f.). These effects cause an equal change at all ΔR_i, which leads to the denominator and therefore U_M to become zero. E.g. temperature changes are therefore self-compensated within the circuit. Ort (1988), p.167f., indicates that, due to production processes, there might be a difference in the temperature behaviour of different production batches. The scatter of one batch is assumed to be small and he gives the standard deviation with 0,25 $\frac{\mu m}{m \cdot K}$, as it rises linear with the temperature. He therefore recommends to use strain gauges of the same packet for this purpose, as it is then fairly certain to get strain gauges of one production batch. Keil (2017), p. 147, points out that the number of the production batch is on each packet.

The temperature-compensation method works only with a compensation gauge at the same location as the corresponding strain gauge used for measurement. To simplify the installation or, if no compensation gauge is needed, the wheatstone bridge itself can be simplified. Therefore, the bridge as shown in Figure 7 with all resistances being strain gauges, is called full-bridge. Some of the strain gauges can be replaced by resistors built in the measurement system. If only one branch of the wheatstone bridge is used, it is called a half-bridge, if only one strain gauge remains, it's called a quarter-bridge (cf. Figure 8). On the one hand, besides the smaller amount of strain gauges, also the cable complexity decreases. Since a full-bridge needs a minimum of 4 cables, a half-bridge needs only three and a quarter-bridge two. On the other hand, also the influence of the strain gauges on the measurement signal is reduced. Therefore, the placement of strain gauges on interdependent locations to increase the measurement signal is reduced (half-bridge) or not possible (quarter-bridge).

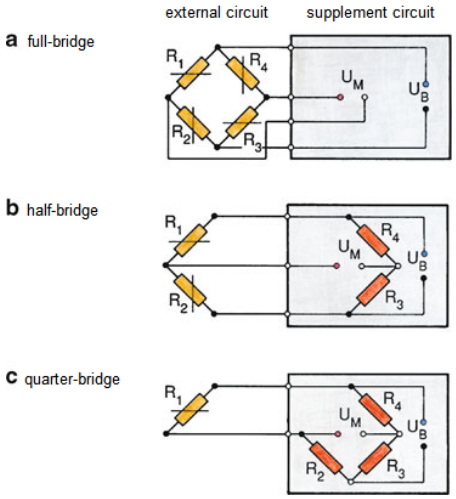

Figure 8: full-, half- and quarter-bridge for measurement with strain gauges
Figure and description taken (and translated) from Keil (2017), p.146, Fig. 4.3

4.2 Cabels

The cables between strain gauge and measurement system are an important part, as they are no ideal conductor. The cables have an ohmic resistance, which, depending on their position in the circuit, can influence the resistance that we want to measure. In addition to that, they have a temperature influence on their resistance. If the measurement is performed by an alternating current instead of a direct current, the capacitance of the cables can cause errors. (cf. Keil (2017), p. 181ff.) The cables to the voltage measurement are negligible, as the input resistance of the voltage measurement is already high-impedant. As the ohmic resistance of cables adds up to the strain gauge resistance, the consequences are different, whether the circuit is configured as a full-bridge or as a quarter- or half-bridge.

At the full-bridge, the resistances of the supply voltage cables are causing some loss in sensitivity of the measurement setup as a whole. Keil (2017)(p. 183) names two factors influencing the sensitivity loss: the cable length and diameter, as these directly influence the cable resistance and the resistance of the strain gauge. The lower the cable resistance and the higher the strain-gauge resistance is, the less loss in sensitivity occurs (cf. Figure 9(a)). Coming from the previously discussed measurements of ice loads on ships, the measurement locations were normally not large in area. Assuming a similar area and a measuring device somewhere near this location, the cable length can be assumed as less than 10 m. Together with strong cables and a higher ohmic resistance of the strain gauges, sensitivity losses of less than 0,1 % are possible. Keil (2017) (p. 183) also states a sensitivity change at changing temperatures, as the cable material (in this case copper) changes its resistance (cf. Figure 9(b)). The changes at the mentioned quantities are rather small and therefore not important. The same goes for the wiring between the strain gauges in the full-bridge, as these cables are negligibly short.

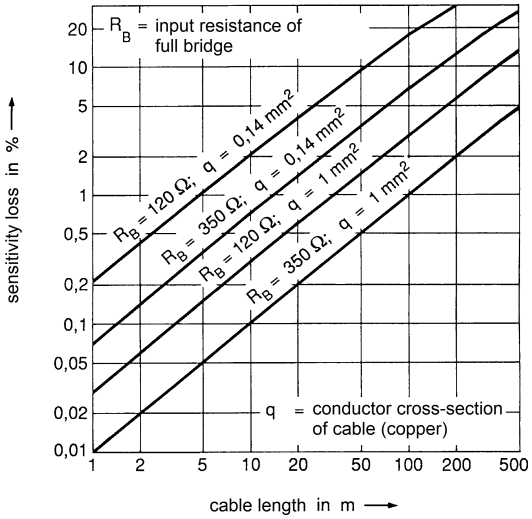

(a) Sensitivity loss due to ohmic resistance of supply voltage cables
figure and description taken and translated from Keil (2017), p. 183

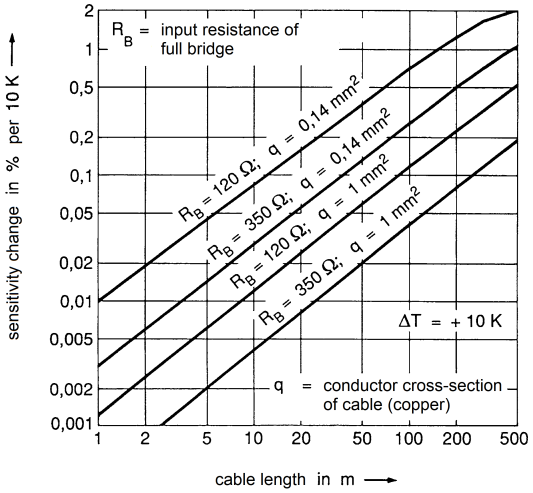

(b) sensitivity change due to temperature change of 10 K
figure and description taken and translated from Keil (2017), p. 184

Figure 9: comparison of cable effects on full bridge strain gauge circuit

Looking at a half-bridge, the change is similar to the full-bridge. But here, the sensitivity loss acts only on one branch of the bridge. On a quarter-bridge configuration, one supply voltage cable and cables in between the resistors influence the measurement. This means, the cable resistance is influencing the strain gauge directly. A temperature compensation, like it is valid for the half bridge and its symmetry of additional resistances at each leg of the branch, is at the quarter-bridge only possible by using 3 cables, like at the half bridge. In this case, the cable to the voltage measurement is separate from the one to R_2 (cf. Figure 8). With the cables at both legs of the branch, the temperature influence is compensated (cf. Keil (2017), p. 184ff.).

Capacitance of cables among each other or to the ground can cause capacitive asymmetry, phase-shifting or amplitude decay (cf. Keil (2017)(p.187)). The measurement errors get considerable, when a carrier frequency of more than 1 kHz and long cables (cf. *ibid*, p. 186) are used. As the frequencies and again the cable lengths used for ice-impact measurement are small, capacitance is no important issue (cf. Keil (2017), p. 186ff., and Riedhof (1974), p.10).

4.3 Electrical circuit

It should be mentioned that the initial circuit of a full-bridge with four cables is generally vulnerable to disturbances, but additional circuit elements can compensate this. For problems with the supply-voltage cables, a six-wire circuit might help; for amplitude decay and phase-shifting the six-cable circuit can be complemented to a two-channel measurement (cf. Keil (2017), p. 193-200). As these methods increase the complexity

of the installation, due to more components in use, and the system, as also the measurement system has more required parts/connections, they are only mentioned in case measurement errors occur.

For half- and quarter-bridges, measurement errors occur at lower cable lengths. Therefore countermeasures are an issue. The Kreuzer-circuit can compensate possible cable influences. It consists of regulators in the measurement system, which has to be fit for this task. The wiring might only need an additional compensation resistance near the strain gauges (cf. Keil (2017), p. 201ff.).

Keil (2017) mentions the protection against electrical and magnetic influences on the circuit. A possible source of this are e.g. motors, generators, transformers or high-oltage lines (cf. *ibid*, p. 206). These kinds of disturbances can occur on a ship in general. If such a disturbance source is in the same room as the measurement system, countermeasures like wire and electronics protection with metal shielding need to be installed. The locations of the measurement site on the hull will most likely not have disturbance sources, therefore the ship structure itself will work as Faraday cage to protect the measurement setup.

4.4 Measurement system

After the cables transported the measurement voltage, this signal has to be processed and the outcoming data saved for analysis. As the raw measurement voltage is in the range of millivolts, this signal has to be amplified (cf. Heringhaus (1982a)). As can be seen in Figure 3, the amplifier also needs a calibration signal for its own calibration. This is important to set the amplifier to a certain measurement range in order to prevent exceeding the maximum gain. Also a zero balance for the zero-strain signal of the wheatstone bridge needs to be set (cf. Keil (2017), p. 215f.). Two procedures are possible: using a stable direct current (DC) or using a frequency- and amplitude-stable alternating current(AC). The direct current seems to be more simple at first, as there is only an amplifier and a power amp at the end. The alternating current uses this current as a carrier frequency, which is transporting the measurement signal. This measurement signal has to be significantly lower than the carrier frequency. In order to get the data, the measured signal needs, after an initial amplification, to go through a demodulator and a low-pass filter, before the power amp produces the wanted measurement values (cf. Heringhaus (1982a)). As the measured signal needs to be lower than the carrier frequency, there is a limit frequency of the signal, resp. a high enough carrier frequency. The limit of a measurable frequency with the DC method is much higher than with AC. Heringhaus (1982a)(p. 45) names momentum processes and impacts as one reason for the use of DC systems, as these produce high frequency measurement signals. In the case of ice impacts on a ship's hull, recent measurements (cf. sections 2.3 and 2.4) have shown rather small frequencies. Even the slope of some impacts as the strain rises and falls again could be seen. Therefore, high frequencies seem not to be important. Additional to that, all the data has to be saved, which is quite a lot, if higher measurement frequencies are used. Long-term measurement already produces a lot of data, therefore, lower frequencies are considered to be sufficient.

If the measurement frequency allows it, the carrier frequency method should always be used (cf. Keil (2017), p. 217). The advantages of this method are less noise and better noise suppression, as well as smaller errors due to disturbances to the system (e.g. electromagnetic fields). Another disadvantage of the DC method is corrosion due to electrolysis in aggressive, humid environment, which can harm the measurement location (cf. Heringhaus (1982b) and Keil (2017)).

The third method, with modern digital technology, is to only have a pre-amplifier module, which also provides the supply voltage and therefore also does the demodulation. After a low-pass filter the signal is digitalized and given to a digital amplifier. A CPU is calculating the amplification and controlling all other parts, like zero balance and calibration (of the pre-amplifier), output data and parameters. Parameters are used to control how the software calculates the amplification and can therefore be easily modified. A change of amplifier properties is possible via software (cf. Keil (2017), p.228ff.).

Keil (2017) (p. 230) mentions as well that the digital amplifier is also much smaller in size and is not lacking at precision compared with analogue amplifiers. Therefore, the choice of amplifier would most likely be a digital one and least likely a DC analogue type.

4.5 Multipoint measurement

There are two ways to measure at many points: one point after the other (serial) or all at the same time (parallel). The serial measurement uses little resources. Only one amplifier is needed, as well as one supplement circuit for completing the wheatstone bridge and simple signal and data management. But the disadvantages are huge. The major disadvantage lies within the principle itself, as not every measurement location is measured at the same time. Dynamic events change during measuring and therefore the measurement data can't be brought together (cf. Keil (2017), p. 235ff.).

The measurement of ice loads is a dynamic event, as an impact happens, and therefore forces on the ships hull vary, move or stop. The structural response in stress and strain in the hull is directly dependent on these impact parameters. Measuring the strain at one point after another will prevent the reverse calculation of the force causing the strain, as the strain of one measurement location doesn't have to add up with the one from the next measurement point. The only acceptable way would be to have a significantly higher measurement rate than the event is changing (cf. Keil (2017), p. 235). Errors would always be made systematically.

Parallel measurement, on the other hand, can be completely synchronized, but the effort in equipment is higher. Every measurement point needs its own channel with amplifier, analogue to digital converter and interface to a computer, which is then collecting and saving all the data. Keil (2017)(p. 239) points out that the data bus transporting the data to the central computer works as a bottle neck at this point. The data rate is dependent on the kind of bus. Also mentioned is the multiplexer as collection method, which by now is replaced by modern analogue/digital converters in every channel (*ibid*, p.240).

5 Parts and composition of measurement system

The possible solutions with all the parameters, limitations and preferences previously discussed now need to be used for the selection of the parts of the measurement setup. As many different varieties are on the market, for different aims of optimization, different solution recommendations can be made. These will be discussed in the following.

As the whole measurement system consists of many parts, it is appropriate to subdivide it into modules:

- The strain gauge in its wheatstone bridge with wiring
- The amplification unit and the computer control with data saving
- The power-supply module

For every module, together with the previously discussed information, solution approaches are to be made. In the end, the modules will be merged together into the complete system solution (cf. Verband Deutscher Ingenieure (1993), p. 9).

5.1 Strain gauge

The aim is to measure location and value of the impact force. As the ship's structure consists of multiple beams supporting the hull plates, these beams take the force and lead them into the whole ship's structure. To analyse the force, we need to know how this structure reacts. Suominen et al. (2017)(p. 161) used a large grillage with clamped sides in his FEA analysis to simulate a section equipped with strain gauges. This is good to get an exact picture of the behaviour of the structure. To explain the possible approaches for measuring the actual impact force, a much simpler model is sufficient. Therefore, I will take a simple beam with the same dimensions that Suominen et al. (2017)(p. 160) also used: frame length = 1,4 m, frame spacing = 0,4 m; web height = 0,2 m; web thickness = 0,019 m(flat bar); hull plating thickness = 0,020 m (Suominen et al. (2017) had an alternating hull plate thickness, but as a simplification I will assume only one thickness). The structural arrangement of one frame and the resulting beam can be seen in Figure 10.

Before performing an actual sample calculation, many things can be seen when looking at classic beam theory. For modelling purposes, a simple beam with hinged supports is assumed. Gross et al. (2011)(p. 175) give a shear and axial force and moment diagram of such a simple beam. It can be seen that the shear force is a constant function with a discontinuity (jump) at the point of the external force acting on the beam. The bending moment is a linear function with a discontinuity (bend) at that same point. The resulting stresses also differ: bending moments cause linear distributed axial stress over the cross-section area, while shear forces cause shear stress (cf. Gross et al. (2012), p. 108ff. and 143ff.). Both result in a strain, which then can be measured with strain gauges. These are two different strategies of measuring the load on the beam.

When aiming for the bending moment, the basic strategy is to use strain gauges, where the axial strain is greatest: on the top or bottom of the beam. Several approaches can

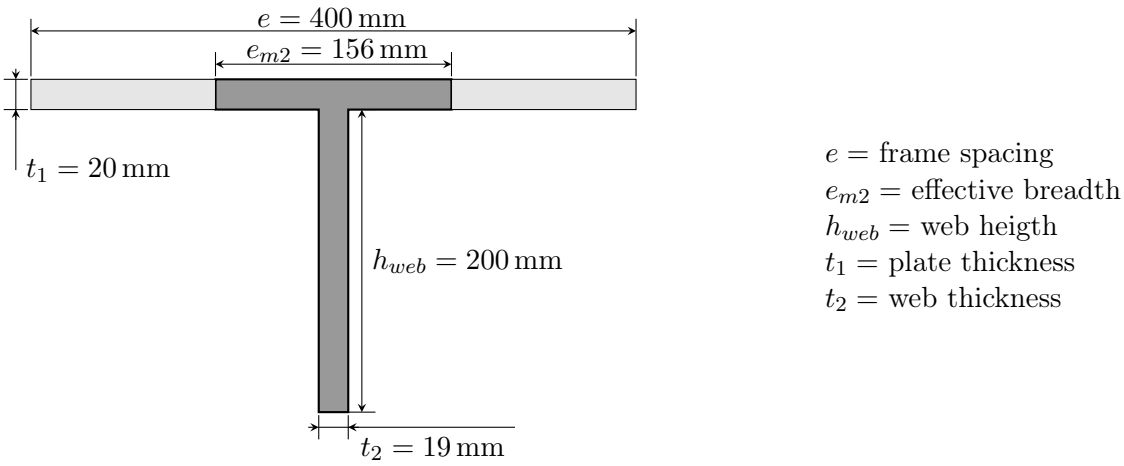

Figure 10: Dimensions of the example T-beam (s. 8.1)

be made for that task. Keil (2017)(p. 151ff.) gives examples with quarter-, half- and full-bridges and the signal $\frac{U_M}{U_B}$ produced in regards to the occuring strains (Indices: Fa = axial force; Fs = shear force; Mb = bending Moment; T = Temperature):

- One strain gauge lengthwise in a quarter-bridge
  without: $\frac{U_M}{U_B} = \frac{k}{4}(\varepsilon_{Fa} + \varepsilon_{Mb} + \varepsilon_T)$ or with: $\frac{U_M}{U_B} = \frac{k}{4}(\varepsilon_{Fa} + \varepsilon_{Mb})$
  temperature compensation gauge.
- Two strain gauges on both sides of the beam in a half-bridge
  $\frac{U_M}{U_B} = \frac{k}{4}(2\varepsilon_{Mb})$
- Four strain gauges on both sides of the beam in a full-bridge
  $\frac{U_M}{U_B} = \frac{k}{4}(4\varepsilon_{Mb})$

These examples give some interesting information: the less strain gauges are used, the less amplification of the signal is achieved just by placing the strain gauges cleverly (cf. Equation (11) and 12). It can also be seen that, in order to get a temperature compensation, the quarter-bridge needs a compensation gauge. Even with this compensation gauge, it still measures strains from any possible, additional axial force, coming from friction between hull and ice. These strains are not what is wanted in the process. Therefore, the compensation gauge could be used better in a half-bridge, which compensates both, temperature and axial strain, and even multiplies the wanted output by two. It is a good mean between the number of strain gauges installed and good quality measurement signals. The only improvement - a full-bridge - enhances the signal, but needs more strain gauges and cables installed. The number of channels used at the measurements system stays the same.

Another problem is that the moment consists of two linear functions (cf. Figure 11e). As the hinged support is only idealized and therefore the support takes a moment into the greater superstructure, two measurement points on each side of the bend in the moment

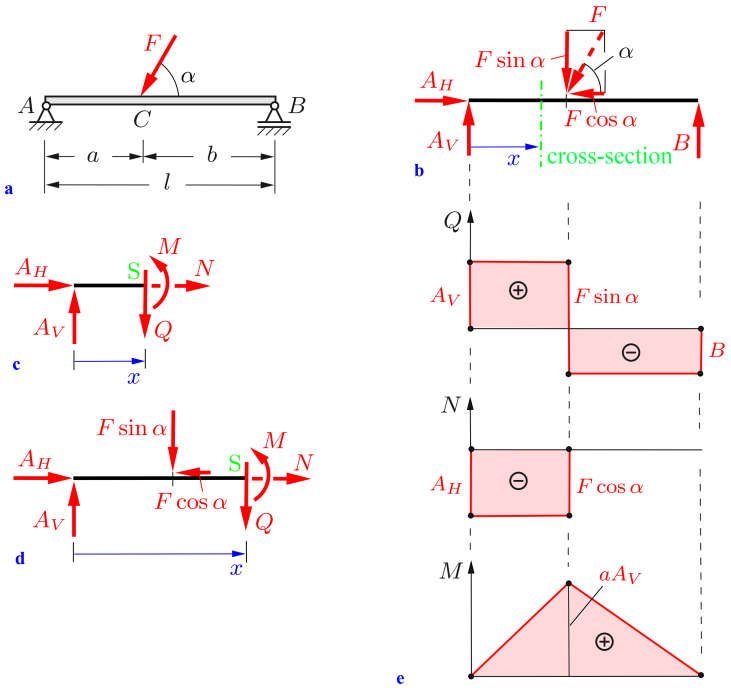

Figure 11: Simple beam with single force
Figure taken and translated from Gross et al. (2011), p. 175, Fig. 7.5

diagram are needed, in order to get the course of the moment functions and - out of it - the force and its position. This is also needed, if the impact force is near to one of the supports. As the two measurement locations would move up closer together, small measurement errors would lead to bigger errors in the moment diagram and therefore in the force calculation. To counteract that, more measurement locations would be needed. A big amount of strain gauges can be seen distributed over a longitudinal frame at Müller and Payer (1988), p. 498, Fig. 2. The result is a bigger effort at this method.

A third problem is that, instead of the example Keil (2017)(p.151) uses, the frame of the icebreaker in my example consists only of the web and a flange as part of the hull plating. This forms a T-beam, which is asymmetrical, and therefore different stresses and strains can be measured at the edge of the web and near the welding to the flange. This would have to be taken into account.

The second method is to measure the strain induced by the shear force. The basic idea is to measure the pure shear strain with two strain gauges with a $+45°$ and a $-45°$ angle to the axis of the beam. Installed in the direction of the principal stress (see Figure 12), one of the strain gauges is therefore lengthened and one is compressed. Keil (2017)(p. 321ff.) gives an example of a measurement device using shear strain at the neutral axis of a short double-T-beam. The assumption also made is that only the web's cross-section area takes the strain of the shear force. Keil (2017)(p.325) gives a full-bridge with one branch on each side of the beam as the measurement setup. Also, at Ritch et al. (2008)(p.

31) measurement, '[e]ach instrumented location consisted of two half bridges, each half bridge is located on the opposite side of the beam or stringer'. Again, an installation using less strain gauges, would be to use a half-bridge on only one side of the beam.

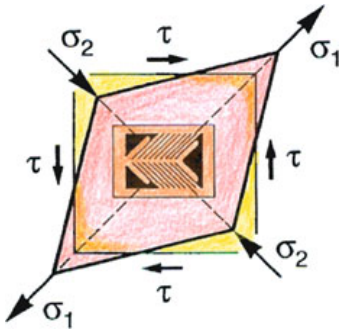

Figure 12: Pure state of shear strain and principal stress
Figure taken from Keil (2017), p. 322, Fig. 10.23

Keil (2017) points out that this is only valid for very idealistic beams without warping. Suominen et al. (2017) used an analytical model with more than one beam with an impact force acting on it involved (resp. the web an the plate as grillage). They assume that the 'loaded frame experiences only a displacement in the loading direction, but the adjacent frames undergo a displacement and rotation' (p. 156), and verify their analysis with a 15,55 kN calibration pull: 'the total loading affecting the frame system is underestimated by 10 % by the analytical method and overestimated by 4 % by the FEA. As the system is scaled to measure significantly higher external loadings, over 1000 kN, and the loadings on the adjacent frames are minor, the results are considered to be good' (*ibid*, p. 164). This leads to the finding that the measurement of stress over shear forces is possible. In the simple beam model, the reason, why this needs less strain gauges as the bending-moment measurement, is easy explainable: The shear force in the beam is a constant function, which only differs at both ends of the beam (cf. Figure 11). By measuring it on both ends, not only the combination of both leads to the total impact force, but their ratio provides insight to the height of the impact (cf. Suominen et al. (2017), p.155f., and Gross et al. (2011), p. 174f.). In addition to that, less strain gauges mean a smaller effort in channels needed at the amplification and computer control unit. A lean system at that point would therefore need less hardware and also use less energy, which has to be stored at the measurement location. This is recommended.

The assumption, the web would be the only part that takes shear stress, made by Keil (2017)(p. 323) is imprecise, therefore the calculation of shear flow T is used to describe the distribution of shear stress τ in the example beam. The approach is to use the definition of shear flow

$$T = \tau \cdot t \tag{13}$$

and how it is influenced by the cross force Q, the first S and second moment of area I

and the flange and web thickness $t(s)$

$$T(s) = -\frac{Q \cdot S(s)}{I}. \tag{14}$$

This leads to the run of τ over the circumferential coordinate s (s. Figure 13)

$$\tau(s) = -\frac{Q \cdot S(s)}{I \cdot t(s)} \tag{15}$$

To use this, the maximum shear stress, resulting in a maximum shear strain, is calculated. It occurs at the neutral axis with an amount of

$$\tau_{max} = \frac{3}{9007\,\mathrm{mm}^2} \cdot Q. \tag{16}$$

The detailed derivation can be seen in Chapter 8.2. This sets the position of the strain-gauge-measurement location to the end of the beam at the neutral axis. The type of strain gauges with $\pm 45°$ is, as mentioned before, possible due to the fact that principal stress acts on the measurement location. Also therefore, the neutral axis is the right spot. The explanation lies within Mohr's circle, which is symmetrical to the τ- and σ-axis and therefore $\sigma_1 = \tau_{max}$ applies (cf. Gross et al. (2012), p. 59). Hooke's law for plane stress $\varepsilon_x = \frac{1}{E}(\sigma_x - \nu\sigma_y)$ gives for principal stress $\sigma_1 = -\sigma_2$

$$\tau_{max} = \frac{E}{1+\nu}\varepsilon_1. \tag{17}$$

Due to this symmetry, $\varepsilon_1 = -\varepsilon_2$ applies, as well as the 90° rotated direction gives τ_{min} analogously. The placing of strain gauges in these two directions makes the strategy of combining them in half- or full-bridges again preferable.

5.2 Amplification unit and computer control with data saving

In order to choose an amplification unit and its properties and settings, it is good to know the range of the expected measurement values. A full-bridge setting will be assumed for now. This results with (1), (12), (16) and (17) in

$$\frac{U_M}{U_B} = \frac{k}{4}4\varepsilon = k \cdot \frac{1+\nu}{E} \cdot \frac{3}{9007\,\mathrm{mm}^2} \cdot Q. \tag{18}$$

The elastic modulus for steel is $E = 2{,}09 \cdot 10^5\,\mathrm{N/mm}^2$ and the Poissons's ration is $\nu = 0,3$; the strain gauges k-factor is assumed with 2 for constantan (cf. Keil (2017), p.33). Therefore, the measurement equation is

$$\frac{U_M}{U_B} = 4{,}1435 \cdot 10^{-9}\,\frac{1}{\mathrm{N}} \cdot Q \tag{19}$$

For an example shear force of 10 kN, this gives $\frac{U_M}{U_B} = 0{,}04\,\frac{\mathrm{mV}}{\mathrm{V}}$. Depending on the ship's location and the expected ice thickness, the measurement range can be adjusted. An overview of different previous measurements is given in 2.1.

The range of products differs a lot. Peekeel, resp. burster gmbh, offers the Autolog 92308, which is a very manifold product, with a lot of options and pre-installations for many measurement channels working synchronously. The problem, as with many commercial products, is that it is designed to be working with a decent power supply. Therefore, most systems of that kind tend to be very power consuming. At this device the minimum option with only 6 channels, an AC-bridge supply voltage and amplifier consumes 75 W with the built-in computer unit (cf. burster gmbh). Within a four-week measurement, this power consumption adds up to 50,4 kWh of energy, which is in the upper range of electric driven car batteries. Therefore, a much smaller power consumption is needed.

An example for a smaller device is HBM's (Hottinger Baldwin Messtechnik GmbH) QuantumX MX1616B. This is an amplifier only, with a total of 16 channels and a power consumption of '<12 W' (cf. HBM(MX1616B)). For the ongoing connection with a data logger and computer-control unit, HBM offers e.g. the module CX22B with a maximum-rated power consumption of '<20 W' (cf. HBM(CX22B)). However, this pretty high power consumption of maximum 32 W allows synchronous measurement at 16 locations. The exactly needed power consumption would have to be found out in a trial, as the specifications only give the upper limit. For the battery consumption and comparison reasons, the maximum power will be assumed for all systems. In this case, it would mean that a battery capacity of $\approx$ 21,5 kWh is required. The power per channel at this system is $\frac{2\,\mathrm{W}}{\mathrm{channel}}$. The solution from HBM is pretty expensive, with 6.840,00 EUR[1] for the MX1616B amplifier and 4.097,35 EUR[2] for the CX22B data module, but therefore the amplifier has a pretty good quality in amplification, resolution of the ADC and low noise.

A promising system on the market is the GSV-6PI from ME-Meßsysteme GmbH. This module is a complete amplifier and data saving unit. It uses the commercial Raspberry Pi 3 together with a digital amplifier module stacked on top of it. The onboard GPIO pins are used for control and the stacked measurement boards provide 6 channels for strain gauge measurement. Since the data sheets[3][4][5][6] are not as detailed as with HBM, its not possible to validate every quality here. The resolution of the ADC is only 16bit instead of 24bit compared to the MX1616B and the resolution steps drop drastically with the rising measurement frequency (cf. Me-Meßsysteme GmbH(GSV6BT)). In our case, as mentioned earlier, the needed frequency for the ice-impact measurement is not that high, therefore, the GSV-6PI is sufficient at this point. Big advantages of this system, however, are the low price of 398 EUR[7] and the low total-power consumption. A request to ME-Meßsysteme revealed that the power supply of the whole board can be realised via the Raspberry Pi (personal telephone call at Me-Meßsysteme, 18 March

[1] Looked up in the HBMshop(MX1616B).
[2] Looked up in the HBMshop(CX22B).
[3] Cf. ME-Meßsysteme (2018b).
[4] Cf. ME-Meßsysteme (2018a).
[5] Cf. Kabelitz (2016).
[6] Cf. Kabelitz (2017).
[7] Looked up in the Me-Meßsysteme GmbH(GSV6PI).

2018). This leads to the maximum power of 12,5 W and therefore a needed maximum energy of 8,4 kWh. This calculation takes only a 6-channel system into account, which means, the power per channel is $\frac{2{,}083\,\mathrm{W}}{\mathrm{channel}}$. Again, the exact consumption, and also the precision of the measurement setup, should be tested beforehand. A problem of this approach might be the small amount of input channels. As the board can not be stacked up further, 6 channels is the maximum, and as an answer to a request, a synchronisation of two of these modules is not designed yet. This would have to be realised on one's own, and since the Raspberry Pi is an open-source platform with the possibility of network building, this should be not too big a problem. As the circuit boards are open on this solution, it is to be mentioned that a casing has to be built or bought.

The last approach in this series from most to least power-consuming-measurement setup would be to use small interfaces (cf. RobotShop inc. (2017)) for each channel and an arduino (with its built in ADC) as data logger (cf. Daouas (2015)). As the specifications of these boards are very thin and the Arduino only provides a 10bit ADC, this approach is very experimental. Due to the low cost of the parts, this might be an option, but also the software for this solution has to be completely examined or written anew. Therefore, this approach might be a bit too low-tech.

As the solutions from ME-Meßsysteme and HBM are pretty even, when it comes to power consumption per channel, they differ in total power consumption, price, precision, and preparatory effort. For a big measurement site (cf. Figure 2, Aft shoulder), the HBM-solution is the better option, because more channels and an easy configurable synchronisation are available. At smaller sites (cf. Figure 2, Bow (shoulder)) the GSV-6PI fits the requirements better. For the operation with not all channels used, the power consumption might drop at both solutions.

To estimate the minimum amount of space needed, the size of one datum has to be calculated. At a measurement frequency of 60 Hz and an overall measurement time of 4 weeks, 145 152 000 points in time need to identified. This requires at least 24bits. Together with 16bits of measured datum and 3bits in order to differentiate the 6 channels, a total amount of 43bits per datum is needed. As computers tend to use bytes, this is round up to 6Bytes. Therefore, number of measured data in 4 weeks is 870 912 000 , which corresponds to 5 225 472 000Bytes $= 5,225$GB. Note that this is a minimum estimation, an 8GB data carrier is recommended.

5.3 Power supply

Since one limitation is to measure in a completely sealed room, all the energy needed for the whole measurement period, would have to be brought into it at the installation and be recharged at every maintenance/data acquisition. As accumulator with high capacity nowadays are based on lithium, these will be the only ones reviewed for this high energy duty.

To get a 10-30 V supply voltage range for the MX1616B and CX22B, a range of accumulators, normally used for solar power and for electrical systems on yachts, provides such voltages. When a 5 V power supply is needed, two main concepts come into mind. The first is to use straightforward 5 V batteries. The second one is to use systems with

a higher voltage and use a step-down module to get to the voltage of 5 V. The use of 5 V batteries comes with some problems. A battery for 8,4 kWh is not commercially available. Therefore, this would have to be assembled from smaller modules. Common big power banks tend to have a range of 20-27Ah, if suitable for the rated output. At 2,5 A, a 26,8Ah battery runs 10,6 h. For a measurement period of 4 weeks = 672hours, 64 of these would be needed, which would cost 53,99EUR[8] ·64 = 3455,36 EUR. The wiring of this solution and the avoidance of any power sink in that wiring could cover a whole new project of electronics. This also is definitely not the specific purpose of power banks. Generally, the cell voltage of lithium based batteries is 3,3-3,7 V, which also limits self-assembled battery banks to ones needing a step-down module and takes a lot of production effort.

Therefore, the mentioned accumulators for solar power and yachting, which normally provide a lot more capacity in single modules at higher voltages, are an option. These also tend to be compatible to one another, as this is often done on yachts. Two examples of that option are the NM-LiFeYPO4-400AH-12V (cf. Nothnagel) and the PYLONTECH LiFePO4 (cf. Bosswerk GmbH & Co. KG). The data sheet of the NM-LiFeYPO4-400AH-12V, gives an operational voltage of 12,8 V, which results, with the 400Ah capacity, in 5,12 kWh. Therefore, two of these are needed in order to get sufficient capacity for the GSV-6PI. The total amount of 10,24 kWh is a good value, as the capacity of a battery gets reduced by several factors, namely low temperatures and the self-discharge (cf. Winston Battery). The PYLONTECH LiFePO4 is a modular battery controlled via LAN (cf. Pylon Technologies Co.). It can be stacked in a rack. The usable capacity is 2,2 kWh per module. Therefore, 4 modules would be too less, 5 with a total capacity of 11 kWh might be enough. Unfortunately, the voltage of this system is in a range of 45-54 V, which means that even the HBM system would need a DC/DC converter.

Even though the data sheet is not very informative about a temperature drop of capacity, it might be in the same range as the NM-LiFeYPO4-400AH-12V. The control unit via LAN, however, could cause some serious power drop over the long time of measurement and increase the self-discharge of the system drastically. The price comparison shows 5900 EUR for the PYLONTECH LiFePO4 with ca capacity of 11 kWh at Bosswerk GmbH & Co. KG and 6996 EUR for the two NM-LiFeYPO4-400AH-12V at Nothnagel. The problems with a control unit, capacity temperature drop and self-discharge will most likely occur also at the 5 V battery packs. And the step-down module can cause an efficiency loss in the power system as well. The higher the difference in DC/DC conversion, the less efficient the step-down regulator works (cf. Texas Instruments (2016)). The efficiency at 48 V/5 V for this step down is at the demanded output current around 78 %. This Texas Instruments (2017) step down has at 12 V/5 V an efficiency of around 90 %.

The recommendation for this module, due to reliability and better fitting voltage range, is the yachting battery version. It supports both systems, the HBM and the GSV-6PI. But it has to be said that the calculation above for this power supply is only valid for 6 locations (resp. 3 frames) of strain gauges with the GSV-6PI. Analogously, the calculation for the HBM system results in five NM-LiFeYPO4-400AH-12V batteries.

[8] Looked up on amazon.de (2018).

6 Recommended Solution

To draw a conclusion, there are many systems out there that are modular fitting together and can therefore be adapted to the user's desires. The focus in this thesis was first to get a long-term self-sufficient system, which means a priority in power consumption. Secondly, the measurement quality has to be sufficient, which leads to a compromise between these two requirements. Long cables are omitted due to the close range of the whole setup to the measurement location, which reduces the complexity of the whole installation. Half- or full-bridge operation has been discussed, and last, but not least, the price was taken into account.

If the budged is not the most important part and/or high precision is required, the HBM solution is recommended. This also counts, if little preparatory work should be done setting up the system, especially at measurement locations with more than 6 strain-gauge-measured points.

The final recommendation of an overall solution is to use high-impedance polimid-sheet-strain gauges in a full wheatstone bridge. This bridge should be located at the ends of the frame in question at the neutral axis with the measurement system in the middle of the measurement location due to short cables. As an amplification and computer-control unit the GSV-6PI from ME-Meßsysteme should be used, and the measurement data can be saved on a data carrier. The power for a four-weeks measurement is provided by two NM-LiFeYPO4-400AH-12V accumulators connected to the measurement system via DC/DC step down converter.

7 Future prospects

As a future prospect to this thesis, the realisation of the recommended measurement solution would be the next step of a long-term ice-load measurement. With respect to some questions resulting from the recommended solutions, the power management is one of the most important. The constant need of power supply over long periods of time causes this problem. The first test trial would be to measure the actual power needed by the recommended systems in the exact configuration for an actual ice-load measurement. The chances are high to achieve a much lower power consumption than the maximum rated, which were used in this thesis as comparison data.

Any reduction in power consumption would mean an increase in constant measurement time, while using the same battery capacity. It should be noted that this is not a linear correlation, as the self-discharge of a battery can't be neglected. Especially at really long measurement periods, a connection to the power generation gets more and more interesting, even if it this increases the installation effort. Also a part-time power supply with batteries as uninterrupted power-supply unit would be conceivable. This would need a charge controller and a battery capacity adjusted to the time period without external power supply.

Another approach to reduce the overall power consumption could be to implement a detection software for ice loads within the computer-control unit of the measurement system. Therefore, most of the time the system could be in a sleep mode and should be activated in strategic periods by a (yet to be designed) clock-control circuit for short ice-detection measurements. This would require an on-board analysis of the data together with a trigger to start the measurement at ice encounter. Such a circuit would need some development concerning electronics and power design. An insight in already existing data of normal ship operation would be needed to estimate ice-encounter start and ending times in order to design the software and the clock control circuit.

8 Appendix

The frame Suominen et al. (2017), (p. 160) described had these dimensions:
1,4 m beam length
0,4 m frame spacing
0,2 m web height
0,02 m hull plating thickness
0,019 m web thickness

8.1 Beam calculation

After the DNV GL (2017) (Part 3 Chapter 12 Section 4, 3.3.4) the effective breadth calculation gives:

$$
\begin{aligned}
l_0 &= 1{,}4\,\text{m} && \text{beam length}\\
l &= 0,6 \cdot 1{,}4\,\text{m} = 0{,}85\,\text{m} && \text{as the support is rather solid}\\
e &= 0{,}4\,\text{m} && \text{frame spacing}\\
\frac{e}{l} &= 2,125 &&\\
\frac{e_{m2}}{e} &= 0,37 + 0,125(0,52 - 0,37) \approx 0,389 && e_{m2} \text{ due to one single load}\\
\Rightarrow e_{m2} &= 0{,}156\,\text{m} && \text{effective breadth}
\end{aligned}
$$

Therefore, the hull and frame can be modelled by a T-beam:
Web: 200×19 mm
Flange: 156×20 mm

The neutral axis z_0 can the be calculated by dividing the first moment of area by the area. The outer part of the flange was used as reference for this calculation. y_0 is at the middle of the web due to symmetry reasons.

	$A[\text{mm}^2]$	$z[\text{mm}]$	$A \cdot z[\text{mm}^3]$	$A \cdot z^2[\text{mm}^4]$	$I[\text{mm}^4]$
Flange	3120	10	31 200	312 000	104 000
Web	3800	120	456 000	54 720 000	12 666 667
$\sum$	6920		487 200	55 032 000	12 770 667

Table 3: Calculation of web and flange properties

$$z_0 = \frac{\sum A \cdot z}{\sum A} \approx 70\,\text{mm}$$

The total second moment of area results by combining the second moment of area to its own centroid with the Steiner's theorem:

$$I_y = \underbrace{\sum I}_{\substack{\text{second moment of}\\ \text{area to centroid}}} + \underbrace{\sum A \cdot z^2}_{\text{Steiner's theorem}} - \underbrace{z_0 \cdot \sum A}_{\substack{\text{Steiner's theorem}\\ \text{for neutral axis}}} = 33\,506\,040\,\text{mm}^4$$

8.2 Shear stress calculations

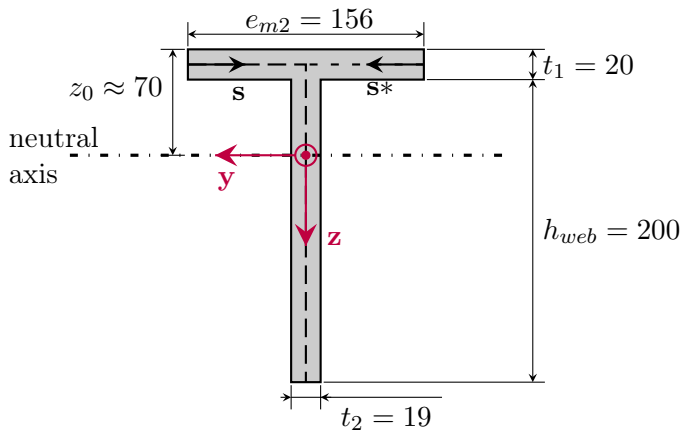

Figure 13: Dimensions of the example T-beam in mm with coordinates:
x, y: beam coordinate system at neutral axis
s: main circumferential shear flow coordinate
s*: side circumferential shear flow coordinate

As can be seen in 15 the run of τ over s is

$$\tau(s) = -\frac{Q \cdot S(s)}{I \cdot t(s).}$$

$$t(s) = \begin{cases} \text{flange:} & t_1 = 20\,\text{mm} \\ \text{web:} & t_2 = 19\,\text{mm} \end{cases}$$

The first moment of area is defined by

$$S(s) = \int_0^s z \mathrm{d}A.$$

The beam can be subdivided into flange and web and is calculated separately. $z_C f$ is the z-coordinate of the centroid of the flange piece. The flange itself is, due to the run of the circumferential shear flow coordinate also subdivided into the main and side coordinate:

$$\text{flange: } S(s) = z_C f \cdot A(s) = -(z_0 - \frac{t_1}{2}) \cdot t_1 \cdot s$$

$$S(s*) = z_C f \cdot A(s*) = -(z_0 - \frac{t_1}{2}) \cdot t_1 \cdot s*$$

Both are symmetrical to the z-axis and are added at the connection to the web. This leads to an axis intercept at first moment of area of the web. Also in the web s is a function of z, therefore

$$\text{web: } S(s) = S(z) = \underbrace{-2(z_0 - \frac{t_1}{2}) \cdot t_1 \cdot \frac{e_{m2}}{2}}_{\text{flange part}} + \underbrace{\frac{z - (z_0 - \frac{t_1}{2})}{2}}_{\text{centroid of web part}} \underbrace{\cdot t_2 \cdot (z + z_0 - \frac{t_1}{2})}_{\text{area of web aprt}}$$

This can then be applied to $\tau(s)$ and as the cross force Q is the quantity in question τ is a function of s and Q:

$$\begin{aligned}
\text{flange: } \tau(s,Q) =& \frac{(z_0 - \frac{t_1}{2}) \cdot t_1 \cdot s}{I \cdot t_1} \cdot Q = \frac{(z_0 - \frac{t_1}{2}) \cdot s}{I} \cdot Q \\
\text{web: } \tau(z,Q) =& -\left(\underbrace{\frac{-(z_0 - \frac{t_1}{2}) \cdot e_{m2}}{I}}_{\text{web part}} + \underbrace{\frac{(z - (z_0 - \frac{t_1}{2})) \cdot t_2 \cdot (z + z_0 - \frac{t_1}{2})}{2 \cdot I \cdot t_2}}_{\text{flange part}} \right) \cdot Q \\
=& \left(\frac{-z_0 - \frac{t_1}{2}) \cdot e_{m2}}{I} + \underbrace{\frac{(z_0 - \frac{t_1}{2})^2 - z^2}{2 \cdot I}}_{\text{max, if } z=0} \right) \cdot Q \\
\Rightarrow \tau_{max}(Q) =& \tau(z=0) = \frac{3}{9007} \cdot Q
\end{aligned}$$

References

amazon.de (2018). Anker PowerCore 26800mAh Power Bank Externer Akku mit Dual Input Ladeport, Doppelt so Schnell Wiederaufladbar, 3 USB Ports für iPhone X 8 8Plus 7 6s 6Plus, iPad, Samsung Galaxy, Android und weitere Smartphones (Schwarz). `https://www.amazon.de/dp/B01JIWQPMW/ref=twister_B077Z3HS9Y?_encoding=UTF8&psc=1` (accessed 19 March 2018).

Bosswerk GmbH & Co. KG (n.y.). PYLONTECH LiFePO4 Speicher 48V - 2,4 kWh. `https://greenakku.de/Batterien/Lithium-Batterien/PYLONTECH-LiFePO4-Speicher-48V-2-4-kWh::572.html` (accessed 18 March 2018).

burster gmbh (n.y.). AUTOLOG: Multichannel-Messystem - easy to use. `https://www.burster.de/fileadmin/user_upload/redaktion/Documents/Products/Brochures/Section_9/BR_AUTOLOG_DE.pdf` (accessed 18 March 2018).

Chalmers, G. F. (1992). Materials, construction, performance and characteristics. In Window, A. L., editor, *Strain gauge technology*, pages 1–38. Elsevier Applied Science, London.

Daouas, B. (2015). Interfacing a Load Cell With an Arduino Board. `https://www.robotshop.com/blog/en/interfacing-a-load-cell-with-an-arduino-board-16247` (accessed 17 March 2018).

DNV GL (January 2017). DNV GL class documents: rules for classification, class programmes, class guidelines and offshore standards.

Gagnon, R. (2008). Analysis of data from bergy bit impacts using a novel hull-mounted external Impact Panel. *Cold Regions Science and Technology*, 52(1):50–66.

Gagnon, R. E. (2001). Surface Load And Pressure Sensing Apparatus: US 6321605 B1.

Gross, D., Hauger, W., Schröder, J., and Wall, W. A. (2011). *Technische Mechanik 1: Statik*. Springer-Lehrbuch. Springer-Verlag Berlin Heidelberg, Berlin, Heidelberg, 11., bearbeitete edition.

Gross, D., Hauger, W., Schröder, J., and Wall, W. A. (2012). *Technische Mechanik 2: Elastostatik*. Springer-Lehrbuch. Springer-Verlag Berlin Heidelberg, Berlin, Heidelberg, 11., bearbeitete edition.

HBM (n.y.a). Datenblatt CX22B-W, CX22B Datenrekorder, b4392. `https://www.hbm.com/fileadmin/mediapool/hbmdoc/technical/b4392.pdf` (accessed 20 March 2018).

HBM (n.y.b). Datenblatt MX1616B, DMS Brücken-Messverstärker. `https://www.hbm.com/fileadmin/mediapool/hbmdoc/technical/b4554.pdf` (accessed 18 March 2018).

HBMshop (n.y.a). 1-CX22B QuantumX Datenrekorder. https://b2bstore.hbm.com/myHBM/app/displayApp/(cpgnum=1&layout=7.01-16_150_6_9_70_34_65_73_131_6&cquery=1-CX22B&uiarea=6&citem=233A0A4E6721194EE1000000AC109934A01D4895C9E81ED59E948EC3B6E9B4DE&carea=233A0A4E6721194EE1000000AC109934&xcm=hbm_b2boccasionalcrm&rdb=0&cpgsize=0)/.do?rf=y (accessed 18 March 2018).

HBMshop (n.y.b). 1-MX1616B QuantumX Brückenmessverstärker (16). https://b2bstore.hbm.com/myHBM/app/displayApp/(layout=7.01-16_150_6_9_70_34_65_73_131&citem=233A0A4E6721194EE1000000AC109934A01D4895C9E81EE69CE554524F0BD27C&carea=233A0A4E6721194EE1000000AC109934)/.do?rf=y (accessed 18 March 2018).

Heringhaus, E. (1982a). Trägerfrequenz- und Gleichspannungs-Meßverstärker für das Messen mechanischer Größen - ein Systemvergleich aus anwendungstecchnischer Sicht: Teil 1: Arbeitsweisen und Vergleich charakteristischer Eigenschaften. *Messtechnische Briefe*, 18(2):42–49.

Heringhaus, E. (1982b). Trägerfrequenz- und Gleichspannungs-Meßverstärker für das Messen mechanischer Größen - ein Systemvergleich aus anwendungstecchnischer Sicht: Teil 2: Verhalten gegenüber externen Störeinflüssen und praktischen Auswahlhilfen. *Messtechnische Briefe*, 18(3):70–73.

Hoffmann, L. (1985). Impact Forces and Friction Coefficient on the Forebody of the German Polar Research Vessel Polarstern. In *The 8th international conference on Port and Ocean engineering under Arctic Conditions, Narssarssuag, Greenland, September 7-14, 1985*, volume 3 of *Proceedings*, pages 1189–1202. Hørsholm.

Kabelitz, H. (2016). ba-gsv-6towamp. https://www.me-systeme.de/produkte/elektronik/gsv-6/gsv-6pi/anleitungen/ba-gsv-6towamp.pdf (accessed 18 March 2018).

Kabelitz, H. (2017). ba-gsv6-signalflow. https://www.me-systeme.de/produkte/elektronik/gsv-6/anleitungen/ba-gsv6-signalflow.pdf (accessed 18 March 2018).

Keil, S. (2017). *Dehnungsmessstreifen*. Springer Fachmedien, Wiesbaden, 2., neu bearbeitete edition.

Kim, H.-S., Lee, C.-J., Choi, K.-S., and Kim, M.-C. (2011). Study on icebreaking performance of the Korea icebreaker ARAON in the arctic sea. *International Journal of Naval Architecture and Ocean Engineering*, 3(3):208–215.

Lee, T.-K., Lee, J.-H., Kim, H., and Rim, C. W. (2014). Field measurement of local ice pressures on the ARAON in the Beaufort Sea. *International Journal of Naval Architecture and Ocean Engineering*, 6(4):788–799.

ME-Meßsysteme (2018a). ba-gsv6pi. https://www.me-systeme.de/product-pdf?product_id=2516&lang=de (accessed 20 March 2018).

ME-Meßsysteme (2018b). Messverstaerker GSV-6PI GSV-6PI. https://www.me-systeme.de/product-pdf?product_id=2516&lang=de (accessed 18 March 2018).

Me-Meßsysteme GmbH (n.y.a). GSV-6PI. https://www.me-systeme.de/shop/de/elektronik/gsv-6/gsv-6pi (accessed 18 March 2018).

Me-Meßsysteme GmbH (n.y.b). Ultraminiatur Messverstärker GSV-6BT. https://www.me-systeme.de/de/technik-zuerst/elektronik/gsv-6/aufloesung-gsv-6bt (accessed 20 March 2018).

Müller, L. and Payer, H. G. (1988). Loads on research vessel polarstern under arctic conditions. In Sackinger, Ph. D., W. M. and Jeffries, Ph. D., P. E., editors, *Port and Ocean engineering under Arctic Conditions*, volume 1, pages 495–508. Fairbanks.

Nothnagel, S. (n.y.). NM-LiFeYPO4-400AH-12V Lithium Batterie Einzelkomponenten Set, Lithium, Li-Ion Akku inkl. BMS u. Sicherheits-Trenn-Relais 250A. https://www.nothnagel-marine.de/product_info.php?info=p3754_NM-LiFeYPO4-400AH-12V-Lithium-Batterie-Einzelkomponenten-Set--Lithium--Li-Ion-Akku-inkl--BMS-u--Sicherheits-Trenn-Relais-250A.html (accessed 18 March 2018).

Ort, W. (1988). Bemerkungen zur neuen OIML-Richlinie IR62: Toleranzen von Folien-DMS-Kenngrößen. In *Experimentelle Mechanik in Forschung und Praxis*, volume 679 of *VDI-Berichte*, pages 161–171. VDI-Verl., Düsseldorf.

Pylon Technologies Co., L. (n.y.). Pylontech LiFePO4 Lithium-Eisenphosphat Batterie US2000 Plus Bedienungsanleitung. https://greenakku.de/download/pylontech_de.pdf (accessed 19 March 2018).

Riedhof, D. (1974). Zur Referenzphaseneinstellung bei Trägerfrequenz-Meßverstärkern. *Messtechnische Briefe*, 10(1):8–10.

Ritch, R., Frederking, R., Johnston, M., Browne, R., and Ralph, F. (2008). Local ice pressures measured on a strain gauge panel during the CCGS Terry Fox bergy bit impact study. *Bergy Bits*, 52(1):29–49.

RobotShop inc. (2017). Load Cell / Wheatstone Amplifier Shield (2ch). https://www.robotshop.com/en/strain-gauge-load-cell-amplifier-shield-2ch.html#Specifications (accessed 17 March 2018).

Rohrbach, C. and Czaika, N. (Dez1959, Feb1960, Mar1960). Über das Kriechen von Dehnungsmeßstreifen unter statischer Zugbelastung I-III. *Archiv für Technisches Messen*, (J135-16, J135-17, J135-18):255–258, 35–38, 55–56.

Ruge, A. C. (1944). Strain Gauge: US 2350972.

Simmons, JR., E. E. (1942). Material Testing Apparatus: US 2292549.

Suominen, M., Karhunen, J., Bekker, A., Kujala, P., Elo, M., von Bock und Polach, Rüdiger, Enlund, H., and Saarinen, S. (2013). Full-Scale Measurements On Boeard PSRV S.A. AGULHAS II In The Baltic Sea. In *The 22nd International Conference on Port and Ocean engineering under Arctic Conditions, Espoo, Finland, Jund 9-13, 2013*, Proceedings.

Suominen, M., Kujala, P., Romanoff, J., and Remes, H. (2017). Influence of load length on short-term ice load statistics in full-scale. *Marine Structures*, 52:153–172.

Texas Instruments (2016). LM5005 High Voltage 2.5 Amp Buck Regulator (Rev. E): LM5005 75-V, 2.5-A Step-Down Switching Regulator With Wide Input Voltage Range. `http://www.ti.com/lit/ds/symlink/lm5005.pdf` (accessed 19 March 2018).

Texas Instruments (2017). TPS54360B-Q1 60 V Input, 3.5 A, Step Down DC-DC Converter with Eco-mode^{TM}. `http://www.ti.com/lit/ds/symlink/tps54360b-q1.pdf` (accessed 19 March 2018).

Verband Deutscher Ingenieure (1993). VDI 2221: Methodik zum Entwickeln und Konstruieren technischer Systeme und Produkte.

Winston Battery (n.y.). Specifications for winston rare earth lithium yttrium power battery WB-LYP200AHA(B). `https://www.nothnagel-marine.de/media/downloads/Lithium_Akkus/Manual%20WB-LYP200AHA%20Winston-Lithium-ion%20Batterie.pdf` (accessed 19 March 2018).

Eidestattliche Erklärung

Hiermit erkläre ich an Eides statt, dass ich die vorliegende Arbeit selbstständig verfasst habe und keine anderen als die angegebenen Quellen und Hilfsmittel benutzt habe. Textpassagen, die wörtlich oder dem Sinn nach auf Publikationen oder Vorträgen anderer Autoren beruhen, sind als solche kenntlich gemacht. Die Arbeit wurde bisher keiner anderen Prüfungsbehörde vorgelegt und auch noch nicht veröffentlicht.

_____ _____

(Ort, Datum) (Unterschrift)